DCA21FA174

POWERPLANTS

Specialist's Factual Report – Attachment 7

Pratt & Whitney DCA21FA174 Metallurgical Investigation Report, July 29, 2022

October 5, 2022

Metallurgical Investigation
Final Report for DCA21FA174

Subject: **Metallurgical Investigation of High Pressure Turbine (HPT) Blades from an accident on July 2, 2021 in Honolulu, Hawaii involving a Boeing 737-200 aircraft, N810TA, operated by Rhodes Aviation Inc., dba Transair Flight 810.**

Date: **July 29, 2022**

Summary and Conclusions:

Review of a full engine set of turbine blades revealed two fractured blades that each could have been primary. Both of the blades were overhauled at least once and were numbered 1 and 6 during engine disassembly. Both blades exhibited chordwise airfoil fractures between 65% span and 75% span.

Examination of the fractured blades found predominantly rough textured, oxidized intergranular fracture surfaces. However, both blades exhibited flat fracture surface regions around the two spanwise holes within the airfoil. SEM examination of these flat regions found very little if any evidence of fatigue, which would be expected to be transgranular and flat.

Metallographic examination of blade 6 found that the flat textured regions were actually in oxidation / corrosion scale, and not sound base metal. More than 75% of the convex wall at hole 1 had been consumed by oxidation / corrosion. Also, many secondary intergranular cracks were observed near the plane of fracture. Based on these observations, it seems likely that internal oxidation / corrosion resulted in loss of load bearing cross section, which resulted in a stress rupture fracture.

1.0 Background

Subject NTSB investigation ID DCA21FA174 occurred at Honolulu, Hawaii on July 2, 2021 at 0145 Hawaiian standard time (HST). The aircraft was ditched in the ocean and both engines were submerged for approximately three and a half months prior to recovery. Per the recommendations of the accident investigators that reviewed the salvaged engine tear-downs, one full engine set of eighty high pressure turbine (HPT) blades from the #2 engine, a JT8D-9A serial number 657227, were submitted for metallurgical investigation.

The blades were numbered 1-80, indicating their relative positions when they were in operation. The engine was reported to have accumulated 101,368 cycles and 70,827 hours since new and 2,085 cycles / 1,055 hours since overhaul. Repair data for the turbine blades was not available, and it was noted that blades had a variety of repair markings. The blades were made of nickel based equiaxed alloy B-1900+Hf, with a two-layer coating system of vapor deposition diffused chromium coating and an outer layer of diffused aluminum coating. B-1900+Hf alloy is known to be susceptible to hot corrosion, and the coating system is intended to provide some measure of protection.

An NTSB materials engineer was present for the initial visual and SEM evaluation of the blades on January 11-12, 2022. Additional work was then completed by PW with remote NTSB oversight.

2.0 Details of Examination

Two blades, numbered 1 and 6, were fractured through the airfoil between 65% and 75% airfoil span. The liberated portions of the blades were not recovered and not available for investigation (**Figures 1 & 2**). During part layout, some debris fell off of the parts onto the white background paper. Four adhesive SEM examination stubs were prepared with a random variety of this debris. All four stubs were examined using a scanning electron microscope (SEM) and energy dispersive spectrometry (EDS). Analysis of multiple regions of these stubs found a variety of compositions. A typical region that exhibited predominantly potassium, calcium, iron rich compositions is presented in **Figure 3**.

It was observed that all of the blades in the set had surface deposits. As some of the deposits covered some of the blade 1 and blade 6 fracture surfaces, it was clear that they occurred post event and as a result of submersion. It was speculated that this was some type of coral or barnacle growth. For the purpose of this investigation, accurate identification of this growth was deemed irrelevant. These deposited organisms will be referred to as barnacles for the remainder of this report, although no biologist was consulted to establish this fact.

2.1 Blade 1

Close up views of blade 1, including concave (CC) side, convex (CV) side, aft side / trailing edge (TE), and forward side / leading edge (LE), are presented in **Figure 4**. The forward root face exhibited the original manufacturer part number, 840001, which was crossed out. A "+" sign was present on the aft root face, indicating a strip and recoat repair of the protective

aluminide coating was performed. A new part number, 840001-003, was engraved on the CC side of the blade platform. A partial serial number was engraved on the CV side of the blade platform, "BKLBBE8," but it was not possible to resolve the terminal 3 digits. The part markings present indicate that the blade had a strip and recoat repair and was reworked to become a -003, but it was not possible to determine when or where these processes occurred.

The fracture surface of blade 1 is shown at increasing magnification in **Figure 5**. Approximately half of the fracture surface was covered with barnacles, however, it was clear that the underlying regions were rough textured. Most of the fracture surface that was not obscured by barnacles was rough-textured and oxidized, which was the result of inter-granular crack propagation and fracture. Under most engine operating conditions, intergranular fracture of this blade alloy is associated with either overstress or stress-rupture crack propagation. Flatter regions of fracture were also present, surrounding the two lightening holes within the airfoil. These holes begin at the outermost span of the blade on the outer diameter end face and run inward until they dead end within the airfoil. These holes were numbered 1 and 2 for reference purposes, with hole 1 being forward and hole 2 being aft. While flat fracture regions can be a result of fatigue progression, which is often transgranular at engine operating conditions, it should be noted that no clamshell-shaped arrest lines were observed. These arrest lines are commonly observed optically at low magnification, even on oxidized fracture surfaces.

Blade 1 was sectioned parallel to the inner diameter (ID) platform at a spanwise location approximately an inch inboard of the fracture surface. The fracture surface was ultrasonically cleaned in a solution of Blue Gold®[1], then rinsed with tap water, dried, and then rinsed with acetone followed by isopropyl alcohol. This cleaning did not remove much if any of the barnacles. The fracture surface of blade 1 was then reviewed using a scanning electron microscope (SEM), at a wide variety of magnifications and using multiple detectors. A low-magnification backscatter electron montage was assembled using ThermoFisher Scientific's MAPS[2] software and is shown in **Figure 6**. Looking down into the holes, it was apparent that the surfaces of these holes were oxidized and contained additional cracks in multiple orientations. Review of the fracture surface found no clear evidence of fatigue, exhibiting either intergranular cracking or smooth textured cracking without fatigue arrest markers at all locations not covered with barnacles. Also, out of plane cracking was observed, which is typically associated with stress rupture fractures (**Figures 7-9**). The images presented were acquired using an Everhart-Thornley detector (ETD) with fully reversed bias. This method of backscatter imaging reduces surface charging caused by non-conductive surface contamination while enhancing topography relative to more conventional backscatter detectors due to the shadowing caused by the angle of the ETD with respect to the fracture surface.

2.2 Blade 6

Multiple views of fractured blade 6 are presented in **Figure 10**. Views from the CV, TE, CC, and LE are included. The aft side of the root face exhibited a "+ orchid" aftermarket repair marking, which indicates that the blade's aluminide coating was stripped and recoated by Turbine Overhaul Services PTE LTD (TOS). The blade was also re-identified from 840001 to

[1] https://www.bluegoldcleaners.com/Our-Products/Blue-Gold-Industrial-Cleaner
[2] https://www.thermofisher.com/order/catalog/product/MAPS2

840001-003, but in a different manner than Blade 1 was re-identified, suggesting that they were processed at different times and or locations. For blade 6, the -003 was simply engraved above the original part number. No evidence of a serial number was observed. The fracture surface of blade 6 was obscured by barnacles more than was blade 1's but was generally similar, with smooth regions around the holes and rough intergranular regions elsewhere.

Blade 6 was sectioned and cleaned using the same procedure described for blade 1, and then the fracture surface was reviewed using SEM. Again, most of the visible fracture features were intergranular, with the exception of a smoother region around each hole. Review of the smoother region found no clear evidence of fatigue, with the possible exception of one small region shown in **Figure 11**. This region could also have been the result of smearing.

A metallographic section was prepared into lightening hole 1 of blade 6 approximately as sketched on the top image of **Figure 12**. This section was reviewed both as polished and in the etched condition using an inverted optical microscope. This review revealed many intergranular cracks in the vicinity of the fracture plane. Also, it was revealed that oxidation / corrosion had consumed more than 75% of the wall thickness on the CV side of hole 1. Based on this analysis, it is clear that the flat regions of fracture surrounding the holes in the blade were the result of cracking of the oxide scale. Review of the section using SEM and EDS found predominantly base metal and base metal oxides. The predominant phases observed decorating the attack front were aluminum oxide and aluminum nitride. A total of eight regions were analyzed by mapping, as shown in **Figure 13**. No evidence of sulfides, which typically exhibit a Ni-Cr-S composition, were observed. Maps from two representative regions are presented (**Figures 14**).

Another metallographic section was prepared into hole 2 of blade 6 approximately as sketched on the top image of **Figure 15**. This section was reviewed both as polished and in the etched condition using an inverted optical microscope. This review revealed many intergranular cracks in the vicinity of the fracture plane. Review of the attack front between the oxide scale and the base metal did not reveal any sulfides. Also, no conclusive evidence of aluminide coating was observed in the plane of polish. The part drawing[3] requires 0.001"-0.004" of aluminide coating on the surface of the lightening holes, also known as "pockets," at the time of manufacture. However, during strip and recoat repair no attempt is made to strip and recoat this region of the part. Instead, this region is supposed to be masked from the repair process. It is not possible now to determine if the parts conformed to the drawing requirement at the time they entered service, nor is it possible to know if the holes were successfully masked during the strip and recoat repair. Also, it is not possible to non-destructively determine if coating is present within the blade lightening holes, so it is very impractical to inspect a large number of blades for this condition.

Per the part drawing[4], the blade attachment region (often referred to as the blade root or fir tree region) of these turbine blades were not aluminide coated at production. These surfaces did not exhibit corrosion. As such, it is reasonable to conclude that saltwater submersion was not responsible for corrosion observed within the lightening holes.

[3] Reference drawing 840001 sheet 1 region D 21-24 and drawing notes 25 and 26.
[4] Reference drawing 840001 sheet 1 region A-23

2.3 Additional Blades

The remainder of the blades were cleaned as much as possible via plastic media blast. However, it was not possible to completely remove all of the barnacles from the airfoil surfaces. The presence of this contamination adds some uncertainty to creep data because the presence of barnacles on part surfaces precluded the use of traditional inspection fixtures for creep measurements. Instead, the blades were 3-D scanned and the resulting data was interpreted using drafting software and some engineering judgement. Results of this exercise are included in Appendix 1. A similar difficulty was encountered with respect to completing Magnetoscop® inspection, because the barnacles prevented full contact of the sensor with the blade surface at some locations. Results of Magnetoscop check are presented in Appendix 2.

Any measurement errors caused by these factors was not of great concern, as the intention of these non-destructive inspections was not to determine conformance to engine manual inspection requirements. These inspections were instead performed to aid in selection of additional blades for destructive analysis. Four blades from the remainder of the set were chosen for additional sectioning based on these Magnetoscop and creep measurements. Blade 28 exhibited low radial creep and low Magnetoscop readings. Blade 30 exhibited high radial creep and low Magnetoscop readings. Blade 31 exhibited low radial creep and high Magnetoscop readings. Blade 43 exhibited high radial creep and high Magnetoscop readings. Inspection results for these four blades are presented in Table 1.

2.3.1 Blade 28

Blade 28 was chosen for further examination because it exhibited both low radial creep and low Magnetoscop readings. Closer views of cleaned blade 28, which was confirmed to be refurbished by TOS similar to fractured blade 6, are presented in **Figure 16**. The highest Magnetoscop locations on the concave and convex sides were circled by the Non-Destructive Evaluation (NDE) group.

Metallographic sections were prepared chordwise through the blade at the span of the marked Magnetoscop locations as shown in **Figure 17**. Review of the metallographic section through the convex side Magnetoscop location revealed oxidation/corrosion less than 0.0032” in depth in the internal holes. Review of the metallographic section through the concave side Magnetoscop location revealed oxidation/corrosion less than 0.006” in depth in the internal holes. The holes did not appear to be aluminide coated (**Figures 18 and 19**). Metal temperature evaluation was completed at approximately 50% and 75% spans. A section was also taken through the root for comparison to baseline microstructure. The microstructure in the airfoil at both 50% and 75% spans was indicative of temperature exposure of at least 2000ºF. Near the LE in the 75% span section, microstructure was indicative of temperature exposure of at least 2050ºF (**Figure 20**). The microstructures observed would not be the expected result of repair processing and are more likely an indication of deteriorating engine health or the result of a single high temperature excursion.

2.3.2 Blade 30

Blade 30 was chosen for further examination because it exhibited high radial creep and low Magnetoscop readings. Closer views of blade 30, which was confirmed to have a "+" similar to blade 1 indicating a strip and recoat, are presented in **Figure 21**. Some of the part markings were illegible. The highest Magnetoscop locations on the concave and convex sides were circled by the NDE group.

Two metallographic sections were prepared chordwise through the blade at the span of each of the marked Magnetoscop locations shown in **Figure 22**. Review of the metallographic section through the convex side Magnetoscop location revealed internal oxidation/corrosion up to 0.020" in depth at the internal hole nearest midchord (hole 2). The forward hole (hole 1) was not visible in the section (**Figure 23**). Review of the metallographic section through the concave side Magnetoscop location revealed internal oxidation/corrosion up to 0.011" in depth at hole 2. The internal hole closest to the LE exhibited less oxidation/corrosion (**Figure 24**). Metal temperature evaluation was completed at approximately 50% and 75% spans. A section was also taken through the root for comparison to baseline microstructure. The microstructure in the airfoil at both 50% and 75% spans was indicative of temperature exposure of at least 2000ºF. Near the LE in the 75% span section, microstructure was indicative of temperature exposure of at least 2050ºF (**Figure 25**).

2.3.3 Blade 31

Blade 31 was chosen for further examination because it exhibited low radial creep and high Magnetoscop readings. Closer views of blade 31, which was confirmed to be refurbished by TOS similar to fractured blade 6, are presented in **Figure 26**. The highest Magnetoscop locations on the concave and convex sides were circled by the NDE group.

Binocular examination of the Magnetoscop location on the convex side of the blade identified a crack-like feature in the spanwise direction (**Figure 27**). The spanwise crack-like feature was broken open. Extensive oxidation/corrosion was observed from the internal hole. The discoloration, indicative of exposure during engine-run time, extended through-wall for at least 0.17" along the surface. Part of the crack was likely sectioned prior to breaking open (**Figure 28**). SEM examination identified features consistent with extensive oxidization/corrosion. The features along the concave wall were consistent with overstress from lab fracture (ductile dimples) (**Figure 29**).

A metallographic section was prepared just outboard of the Magnetoscop location (outboard of where the crack was located). The locations of the highest convex and concave Magnetoscop readings were at approximately the same span so only one section was prepared (**Figure 30**). On the hole closest to the LE, the oxidation/corrosion extended up to 0.043" through the CC wall, approximately 2/3 of the wall thickness. The oxidation/corrosion measured less than 0.007" on the hole closer to midchord (**Figure 31**). Metal temperature evaluation was completed at approximately 50% and 75% spans. A section was also taken through the root for comparison to baseline microstructure. The microstructure in the airfoil at both 50% and 75% spans was indicative of temperature exposure of at least 2000ºF. Near the LE in the 75% span section, microstructure was indicative of temperature exposure of at least 2050ºF (**Figure 32**).

2.3.4 Blade 43

Blade 43 was chosen for further examination because it exhibited high radial creep and high Magnetoscop readings. Closer views of blade 43, which was confirmed to be refurbished by TOS similar to fractured blade 6, are presented in **Figure 33**. Some of the part markings were illegible. No part markings were observed on the platform. The highest Magnetoscop locations on the concave and convex sides were circled by the NDE group.

Metallographic sections were prepared chordwise through the blade at the span of the marked Magnetoscop locations as shown in **Figure 34**. Review of the metallographic section through the concave side Magnetoscop location revealed internal oxidation/corrosion up to 0.018" in depth (**Figures 35**). Review of the metallographic section through the convex side Magnetoscop location revealed internal oxidation/corrosion up to 0.022" in depth (**Figures 36).** Metal temperature evaluation was completed at approximately 50% and 75% spans. A section was also taken through the root for comparison to baseline microstructure. The microstructure in the airfoil at both 50% and 75% spans was indicative of temperature exposure of at least 2000ºF. Near the LE in the 75% span section, microstructure was indicative of temperature exposure of at least 2050ºF (**Figure 37**).

2.3.5 Blades 5 and 80

These two blades were positioned adjacent to fractured blades 1 and 6, in the positions where the direction of rotation makes secondary damage more likely. Both of these blades exhibited shroud fractures, which appeared to be secondary. Both fracture surfaces were rough textured and shiny, suggesting they were caused by overstress and was not exposed hot gases for much time (**Figures 38 and 39**).

Blade		Radial Creep Measurement	Magnetoscop readings after cleaning	
Blade	**Side**		**Model 1.070**	**Model 1.069**
28	CC	0.0028”	1.002	1.004
	CV		1.000	1.001
30	CC	0.019”	1.003	1.007
	CV		1.003	1.006
31	CC	0.008”	1.056	1.112
	CV		1.057	1.114
43	CC	0.0193”	1.032	1.064
	CV		1.043	1.086

Table 1: Non-destructive creep inspection and Magnetoscop[5] inspection measurements used to select four additional blades for destructive analysis.

[5] Model 1.07 is the model of Foerster Magnetoscop currently available, and model 1.069 is a discontinued model called out by the engine manual. These instruments measure relative permeability μr in accordance with IEC 60404-15 and ASTM A342M.

Figure 1: Blade set viewed from convex (suction) side of airfoils. The two indicated blades, #1 and #6, were fractured between 65 and 75 percent span.

Figure 2: Blade set viewed from concave (pressure) side of airfoils. Two blades, #1 and #6, were fractured.

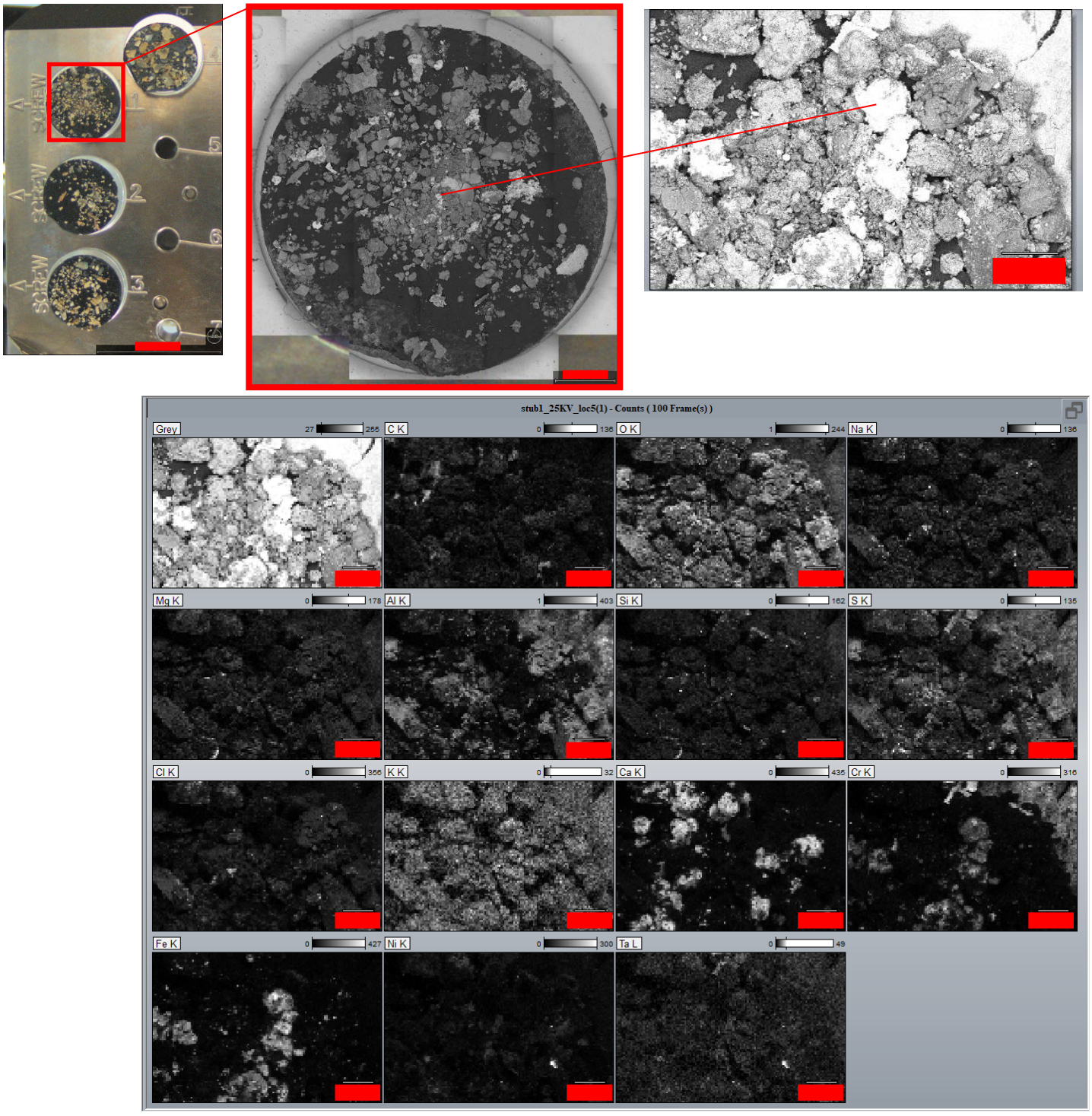

Figure 3: Elemental mapping of a typical region containing multiple particles of debris that fell off of the parts during layout found predominantly potassium, calcium, iron rich compositions.

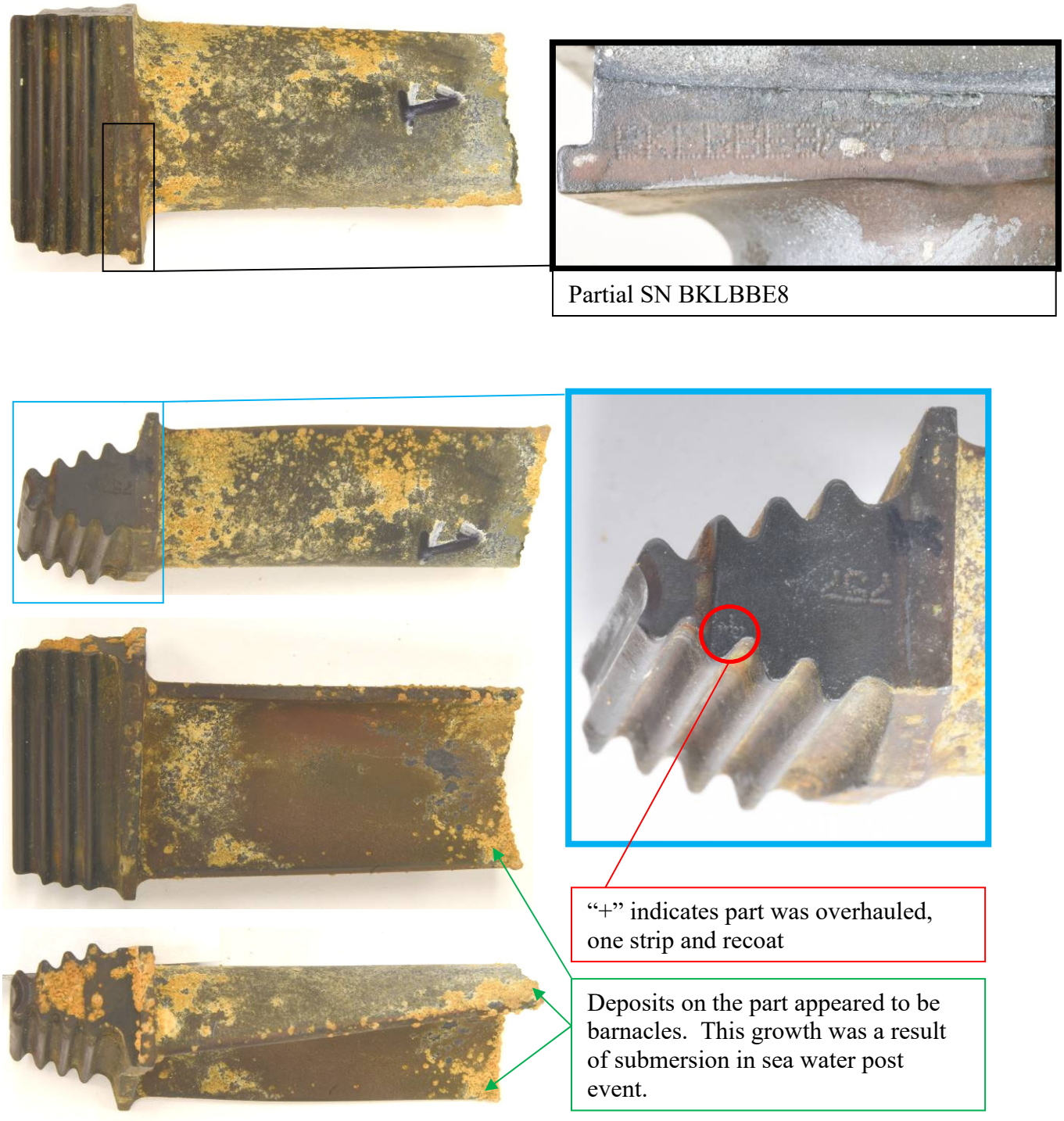

Figure 4: Closer views of fractured blade 1, which was confirmed to be refurbished. Views from top down are CV, TE, CC, and LE, respectively.

LE (Forward>)

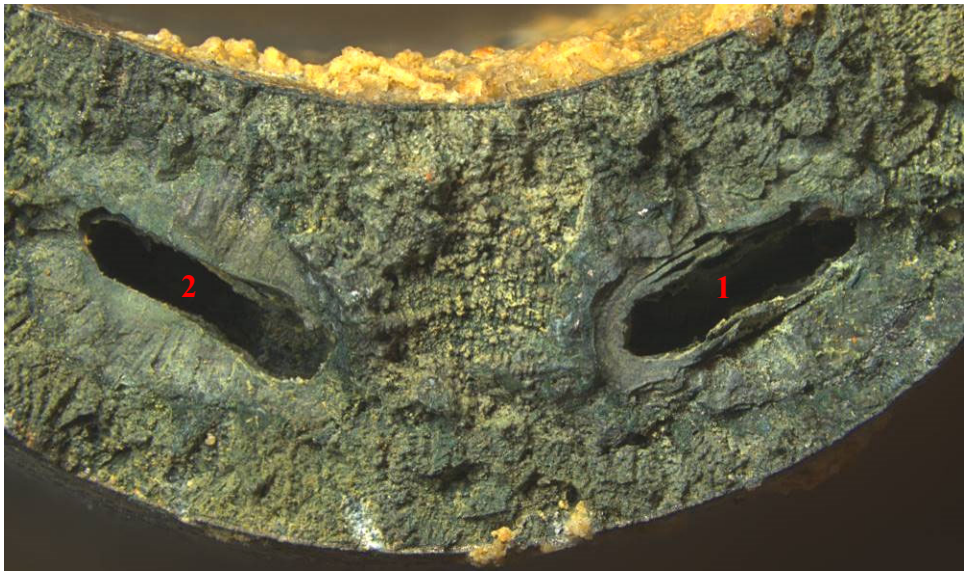

Figure 5: Optical images of the fracture surface of blade 1. Regions of the surface not covered with ocean deposits were predominantly rough textured (intergranular), with the exception of the regions around the holes, which were mostly flat. The holes were labeled 1 and 2 from front to back for ease of reference.

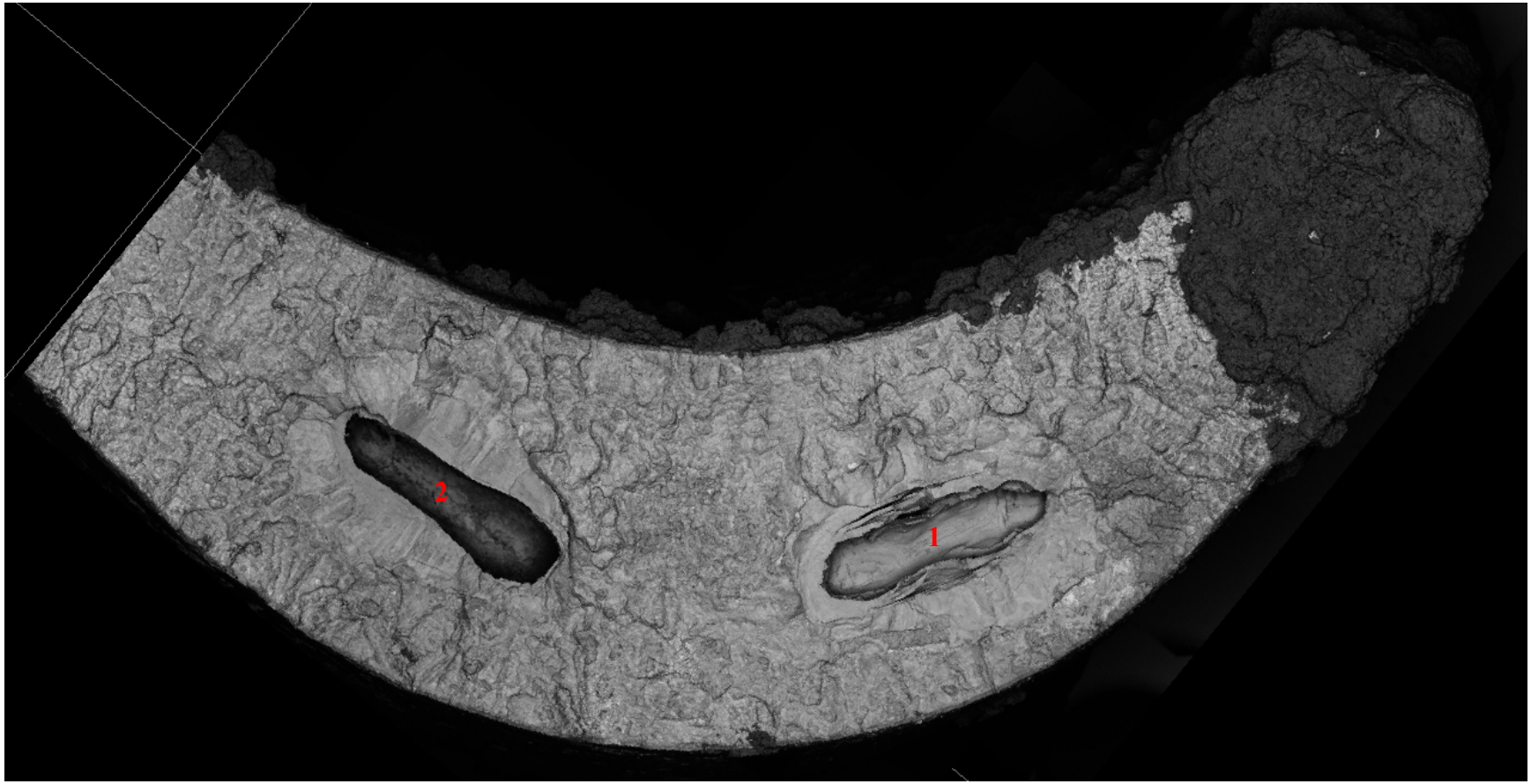

Figure 6: SEM backscatter electron (BSE) montage of blade 1 fracture surface. Note, some stitching errors may be present. Re-oriented images at higher magnification follow.

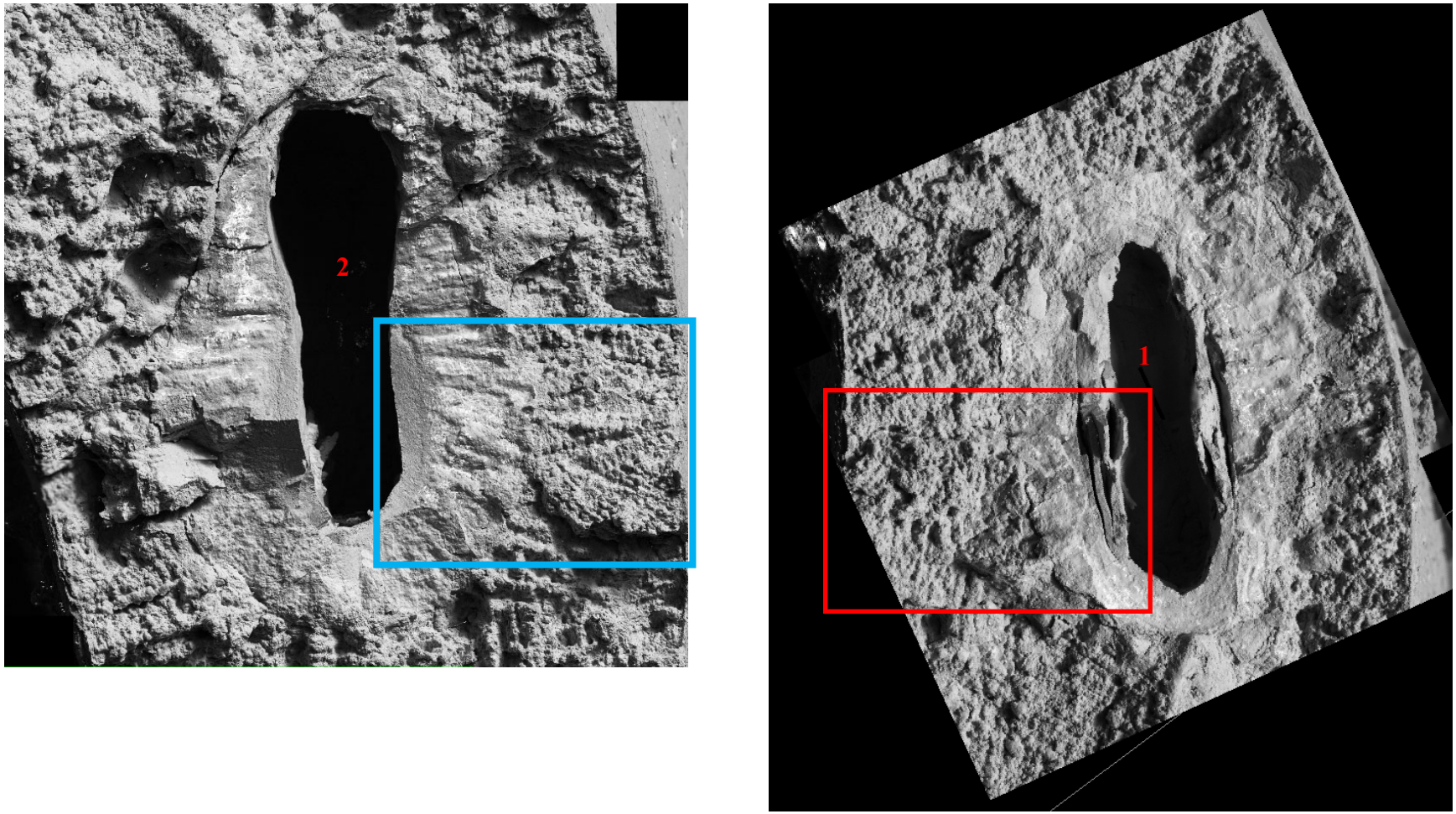

Figure 7: Everhart-Thornley detector (ETD) BSE montages of blade 1 fracture surface at holes 1 and 2. Texture around the holes was relatively flat, while texture elsewhere was intergranular. Close-up images of the regions enclosed in red and blue rectangles follow.

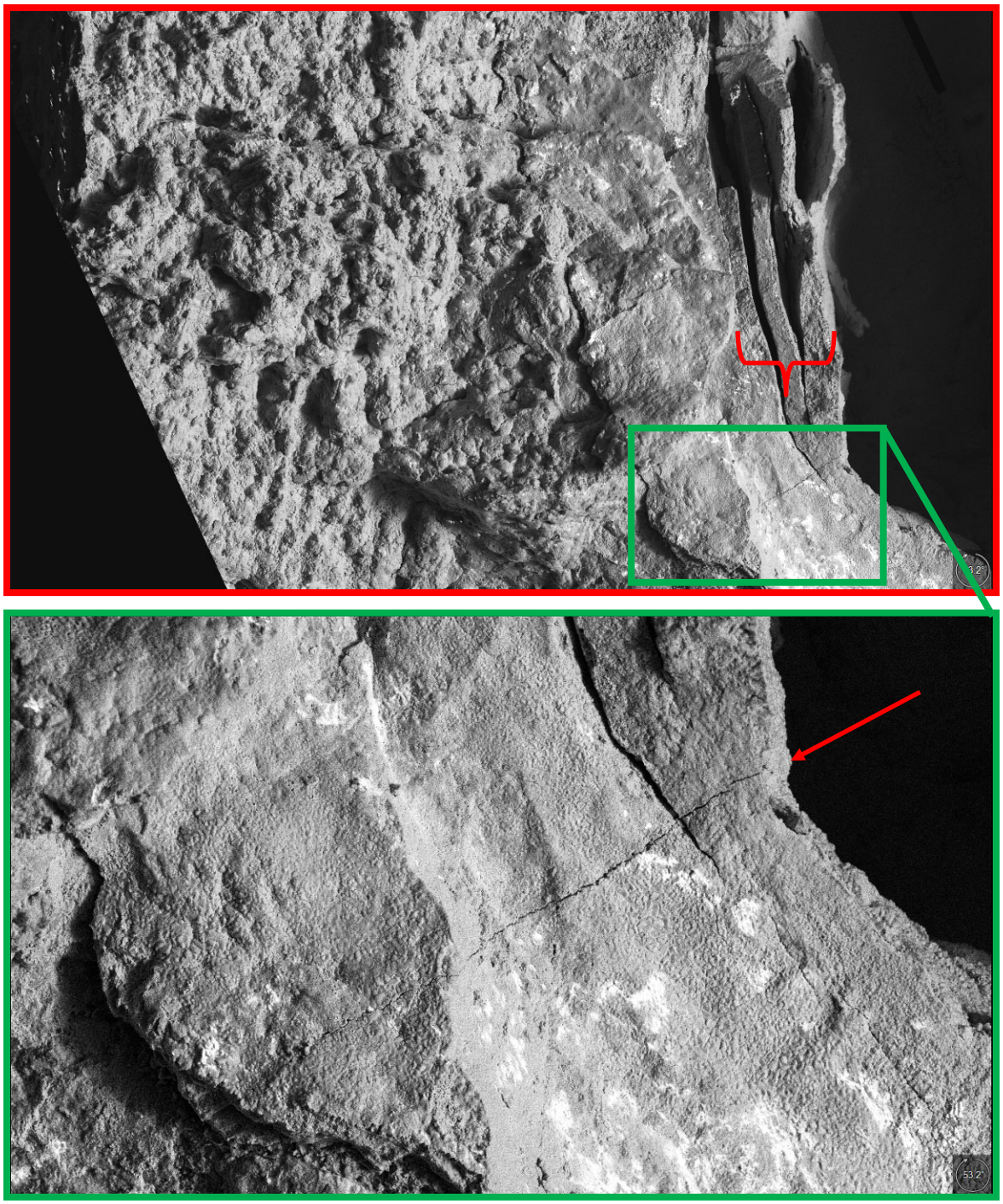

Figure 8: ETD BSE images of blade 1 fracture surface (refer to Fig. 6, red rectangle). Upper image reveals stratified layers at hole surface, as indicated with a red brace. The lower image shows the relatively flat texture at the hole, as well as an out of plane crack (red arrow). No fatigue markers or river lines were apparent.

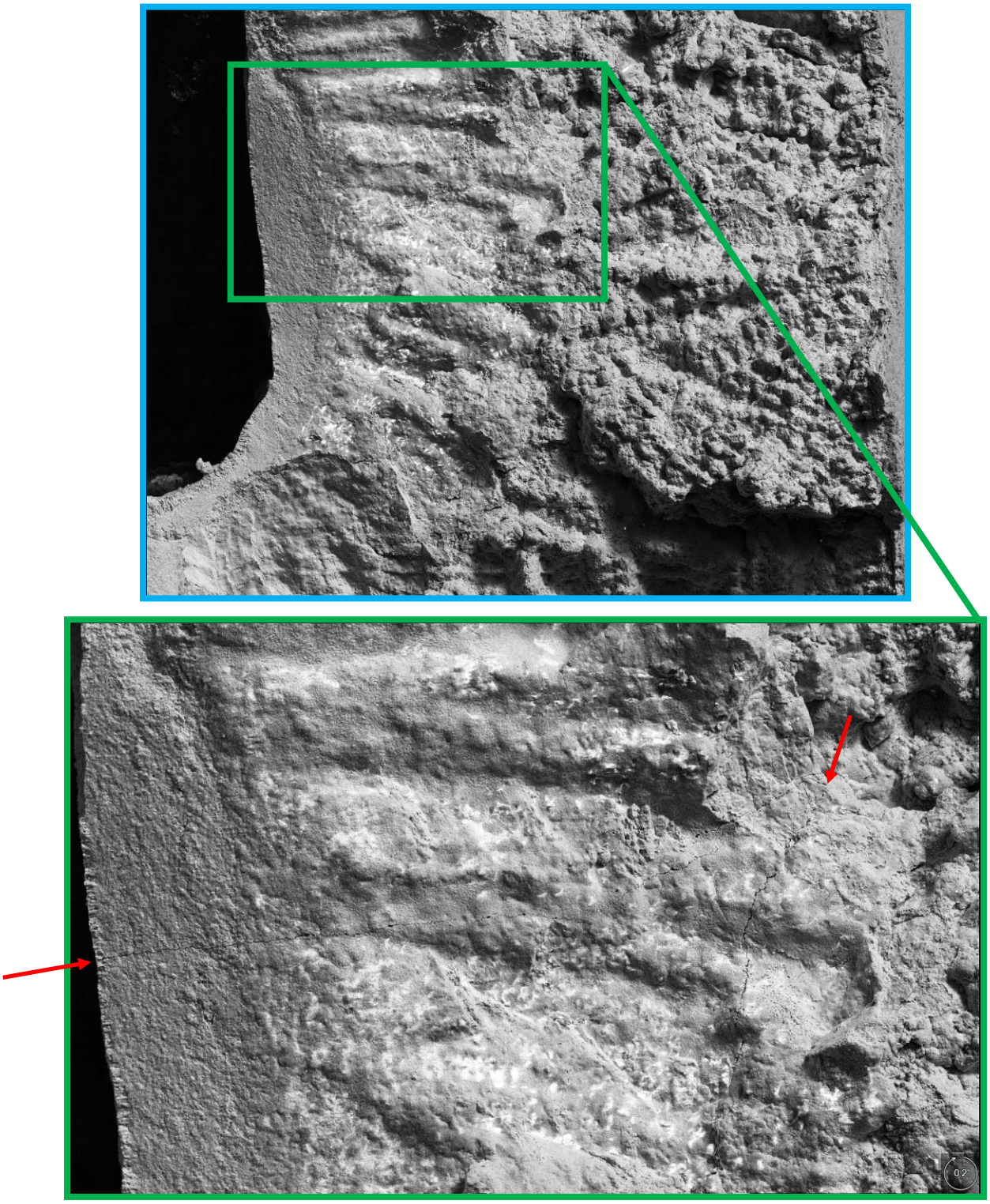

Figure 9: ETD BSE images of blade 1 fracture surface (refer to Fig. 6, blue rectangle). Upper image shows both smooth and intergranular fracture. The lower image shows the relatively flat texture at the hole, as well as two out of plane cracks (red arrows). No fatigue markers or river lines were apparent.

Figure 10: Closer views of fractured blade 6, which was confirmed to be refurbished. Views from top down are CV, TE, CC, and LE, respectively. The fracture surface of blade 6 was obscured by barnacles more than was blade 1's, but was generally similar with smooth regions around the holes and rough intergranular regions elsewhere.

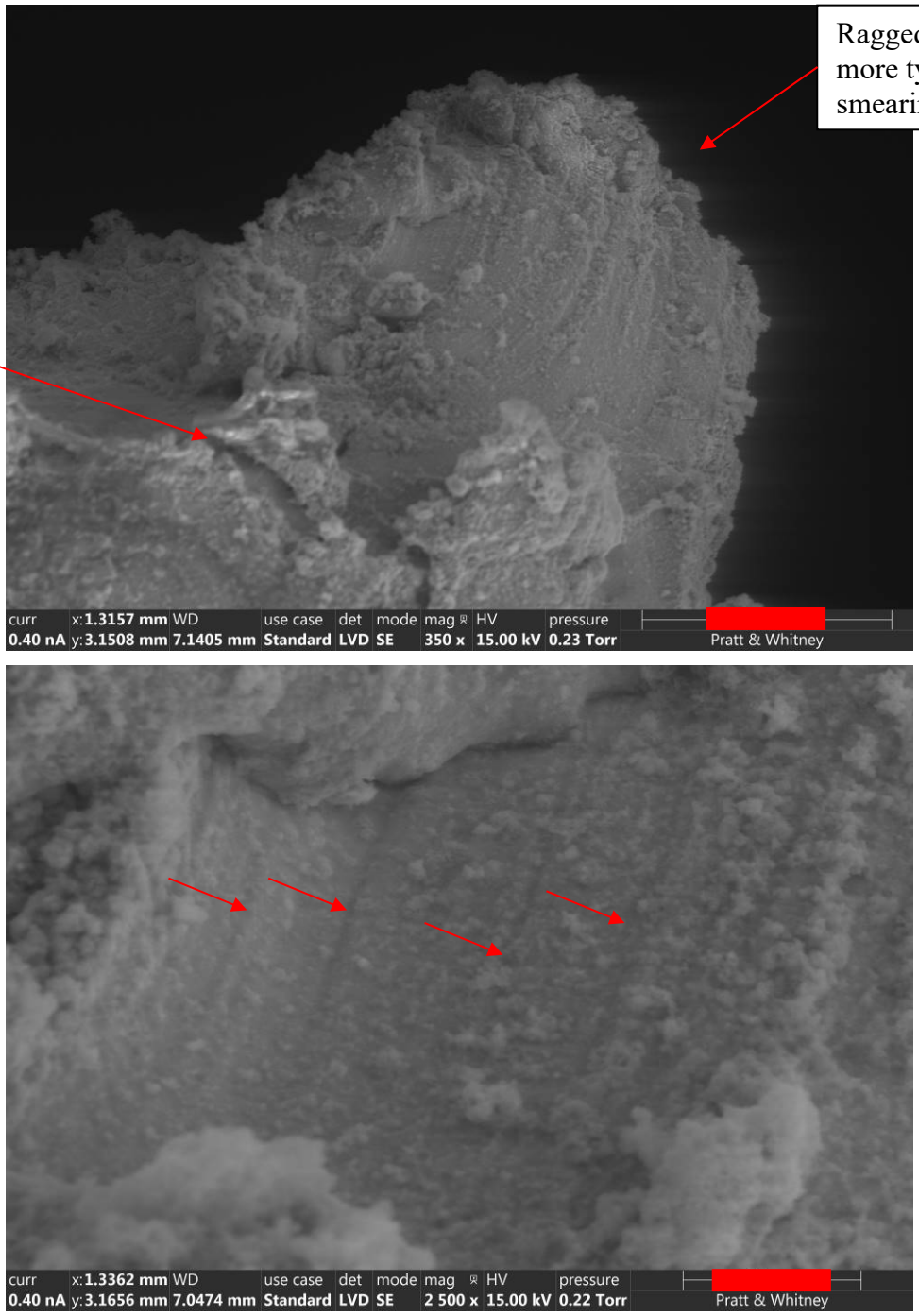

Figure 11: The images above taken from blade 6 around hole 2 were inconclusive. Features indicated in the top image suggest smearing, while feint plastic deformations of the crack surface indicated in the bottom image could be evidence of fatigue.

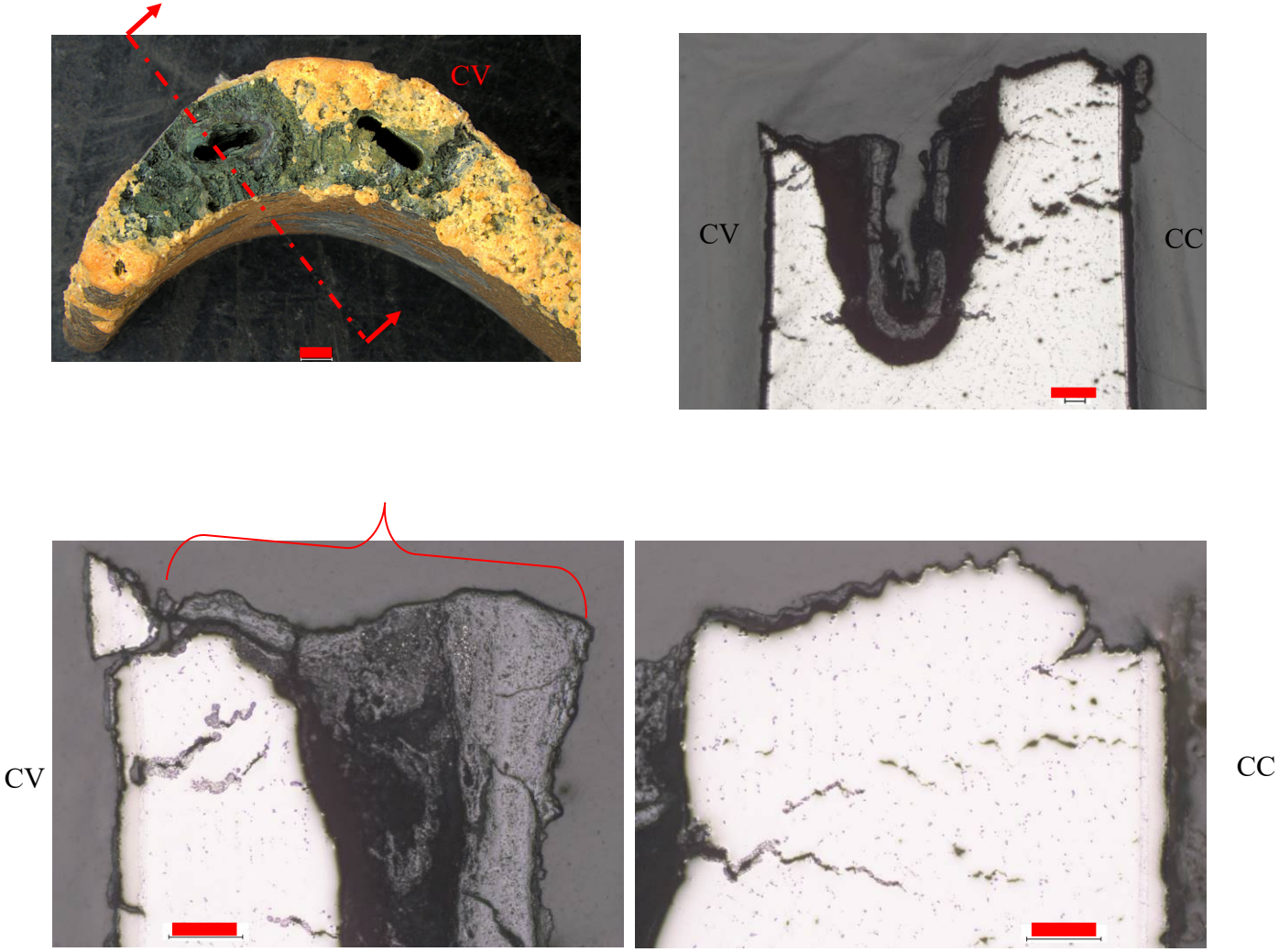

Figure 12: Metallographic review of Blade 6, hole 1 revealed multiple intergranular cracks near the fracture plane. Also, the CV wall was predominantly consumed by oxidation / hot corrosion at the fracture plane (red brace).

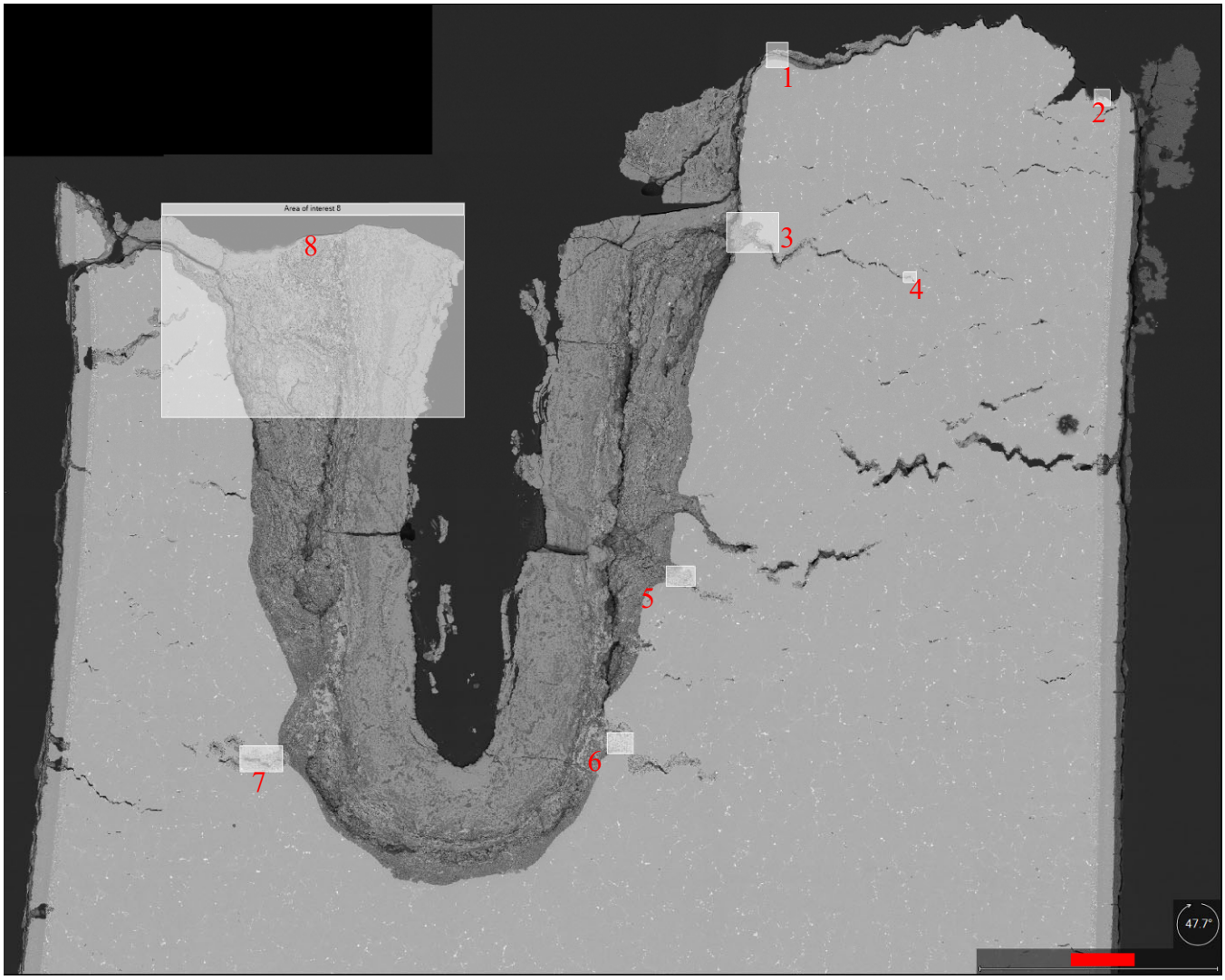

Figure 13: SEM metallographic review of Blade 6, hole 1. EDS Mapping was used to analyze the elements present within each of the regions enclosed in rectangles above. Results of this analysis follow.

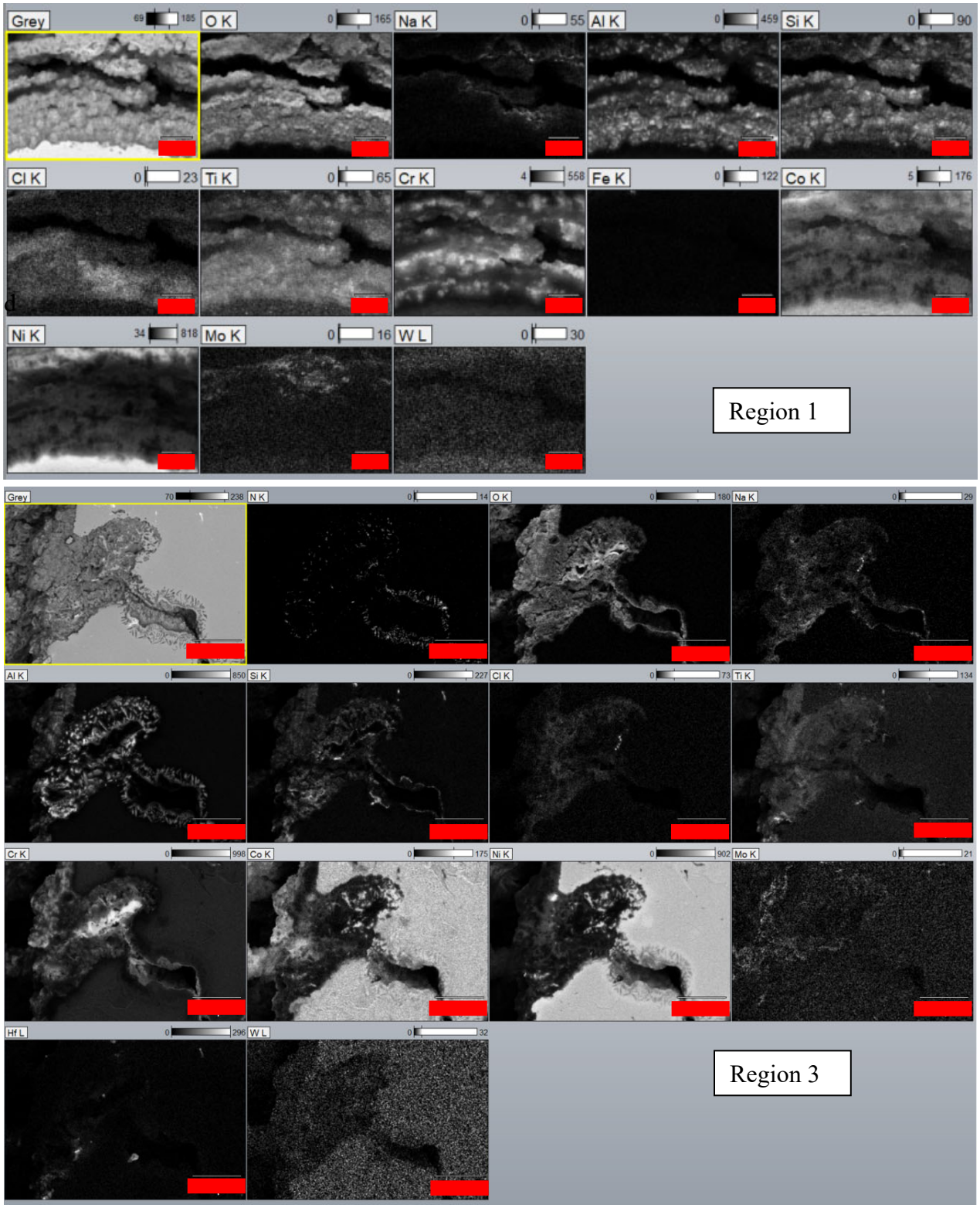

Figure 14: SEM metallographic review of Blade 6, hole 1. EDS net count maps of regions 1 and 3 revealed predominantly base metal and base metal oxides, with aluminum oxide and aluminum nitride decorating the attack front. No evidence of sulfidation was found.

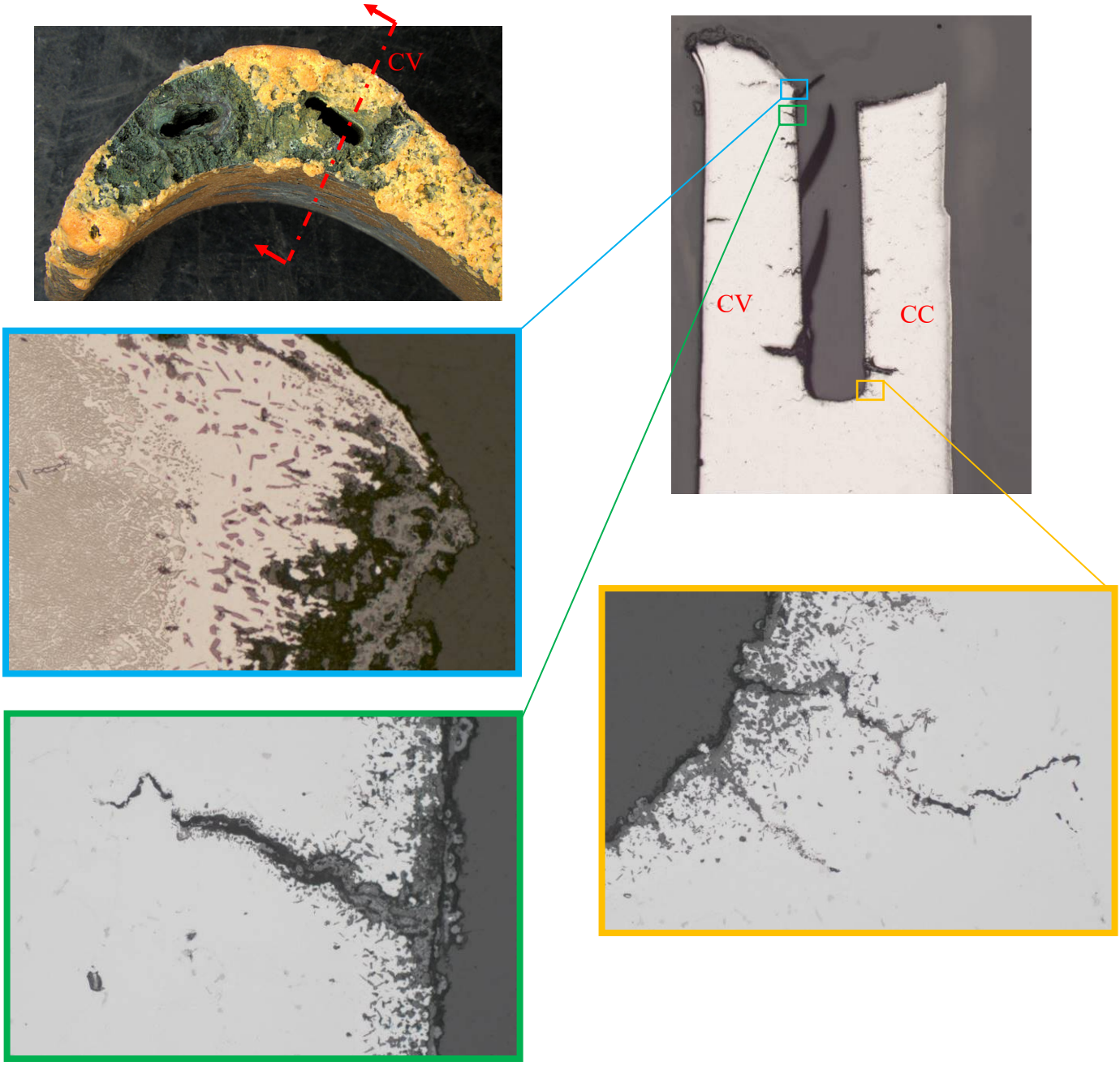

Figure 15: Metallographic review of Blade 6, hole 2 revealed multiple intergranular cracks near the fracture plane. Higher magnification views of secondary cracks and oxidation / corrosion attack are also shown.

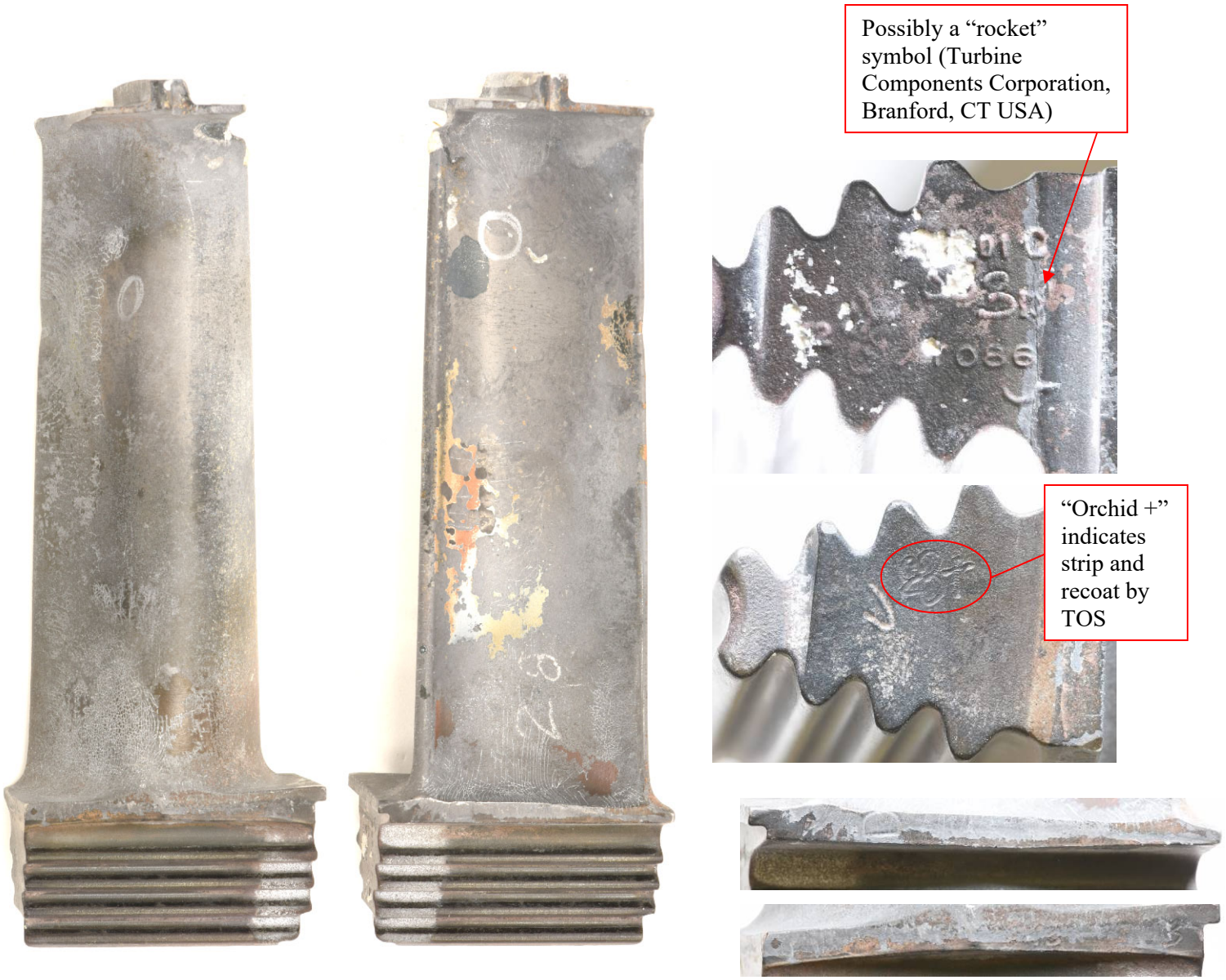

Figure 16: Closer views of blade 28 after cleaning, which was confirmed to be refurbished by TOS. Images showing the CC and CV sides as well as the part markings. Some of the part markings were obscured by coral or barnacle growth, even after cleaning. The highest Magnetoscop locations on the concave and convex sides were circled by the NDE group.

Figure 17: Images showing the locations of the metallographic sections prepared through the highest Magnetoscop readings on the concave and convex sides of blade 28.

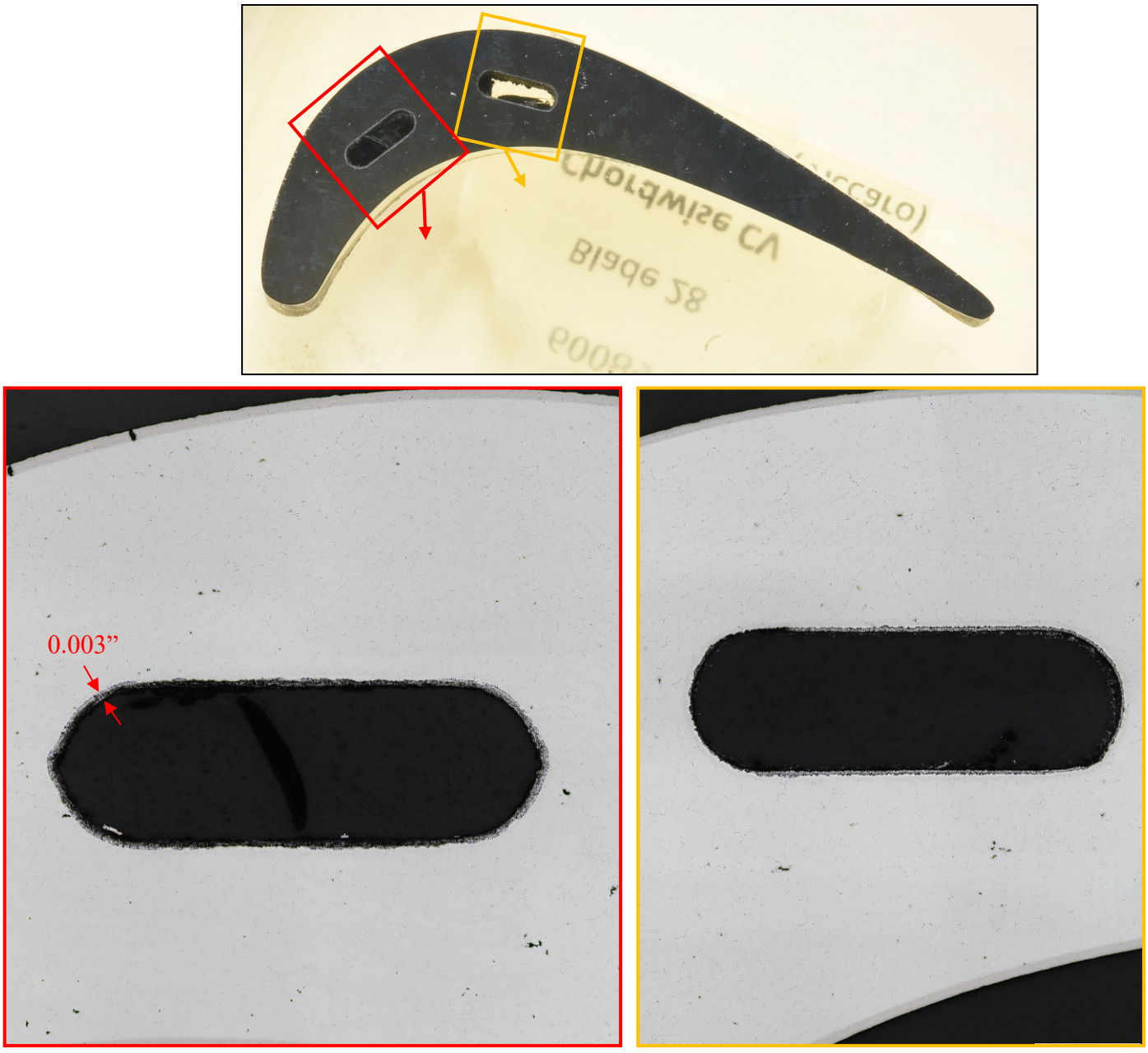

Figure 18: Metallographic review of the section through the convex side Magnetoscop location on blade 28 revealed internal oxidation/corrosion less than 0.003” in depth. The internal surfaces of the holes did not appear to be coated.

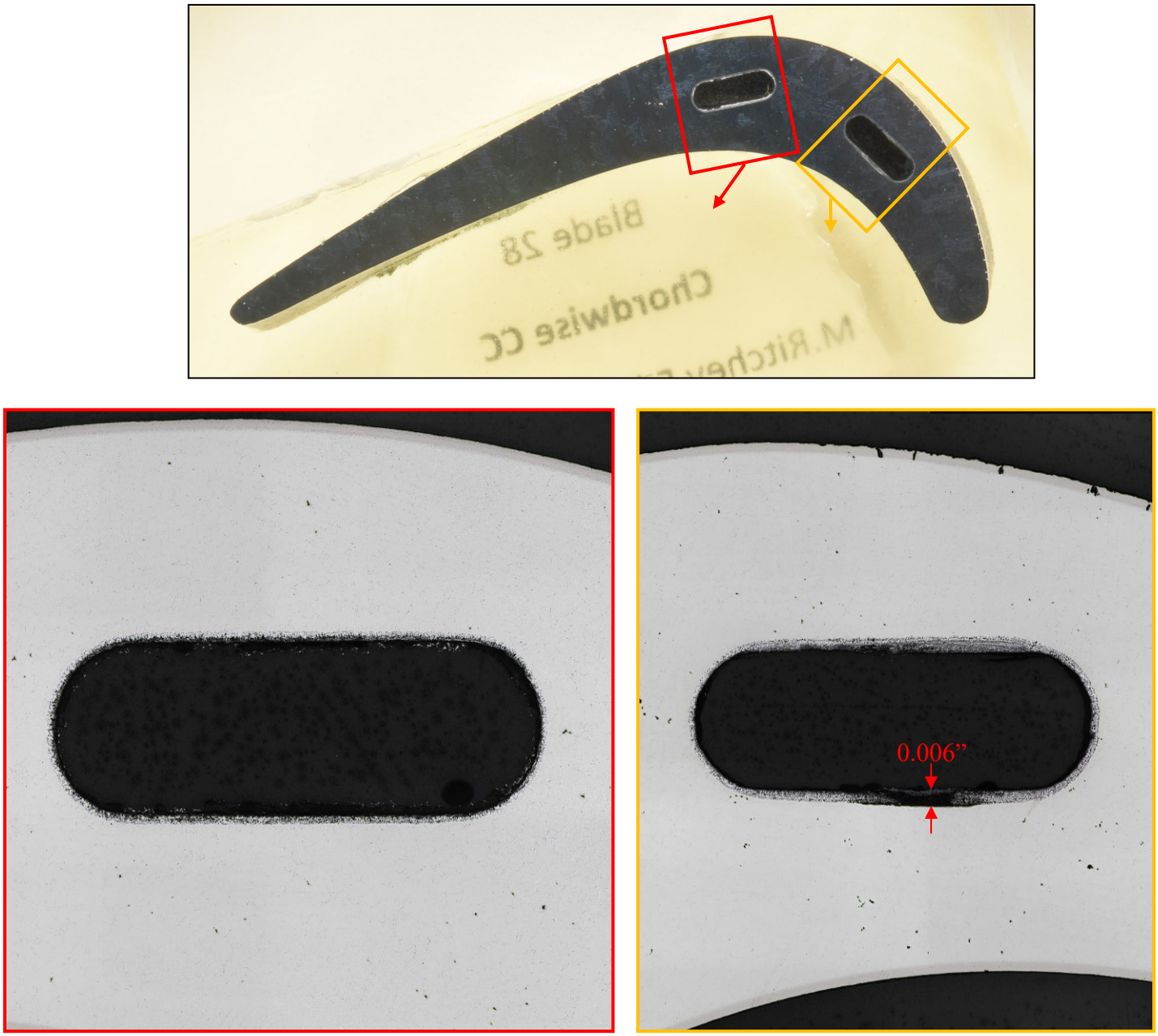

Figure 19: Metallographic review of the section through the concave side Magnetoscop location on blade 28 revealed internal oxidation/corrosion less than 0.006”. The internal surfaces of the holes did not appear to be coated.

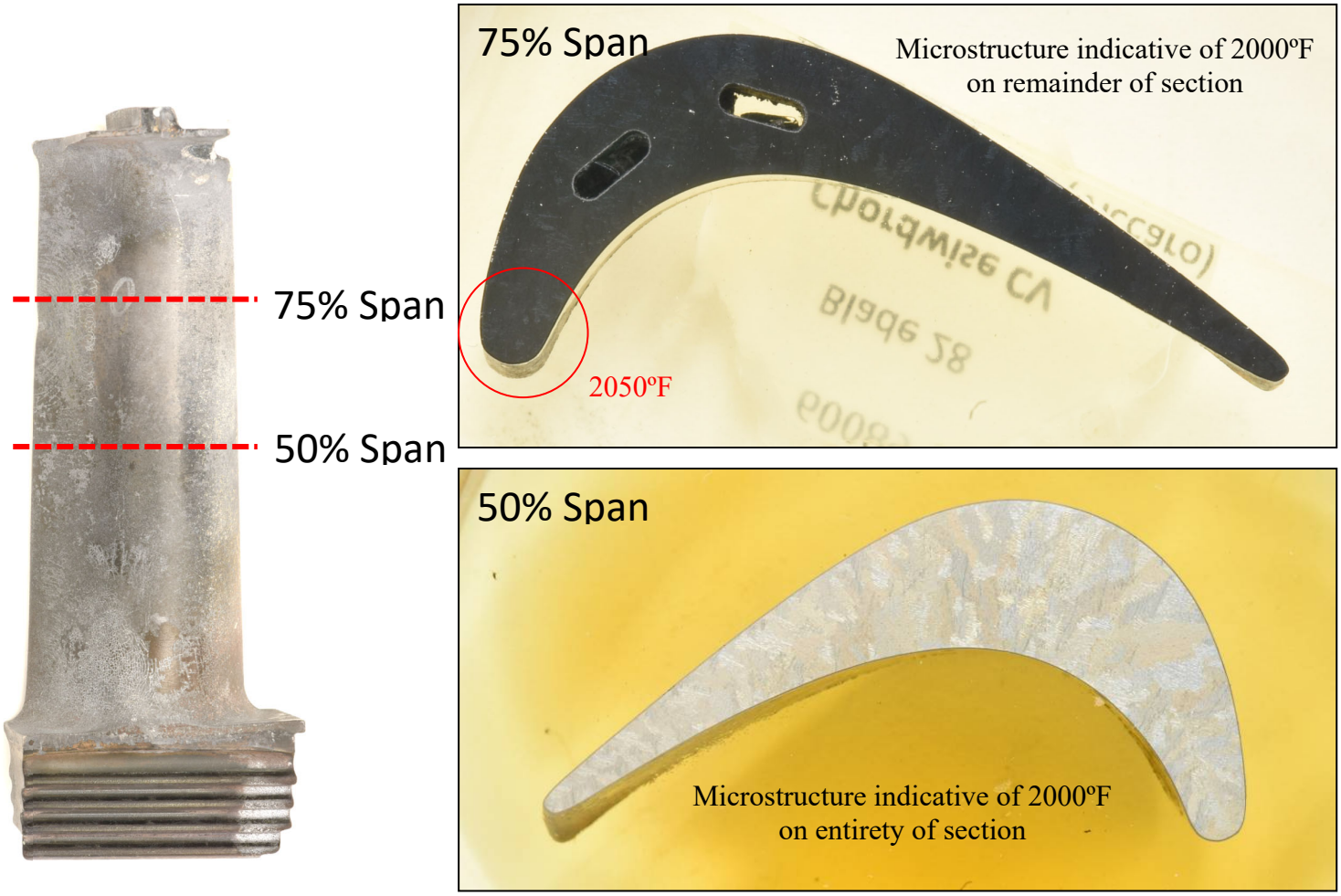

Figure 20: Metal temperature evaluation was completed at approximately 50% and 75% spans on blade 28. The microstructure in the airfoil at both 50% and 75% spans was indicative of temperature exposure of at least 2000ºF. Near the LE in the 75% span section, microstructure was indicative of temperature exposure of at least 2050ºF.

Figure 21: Closer views of blade 30 after cleaning, which was confirmed to be refurbished. Images showing the CC and CV sides as well as the part markings on the root and platform. Some of the part markings were illegible. The highest Magnetoscop locations on the concave and convex sides were circled by the NDE group.

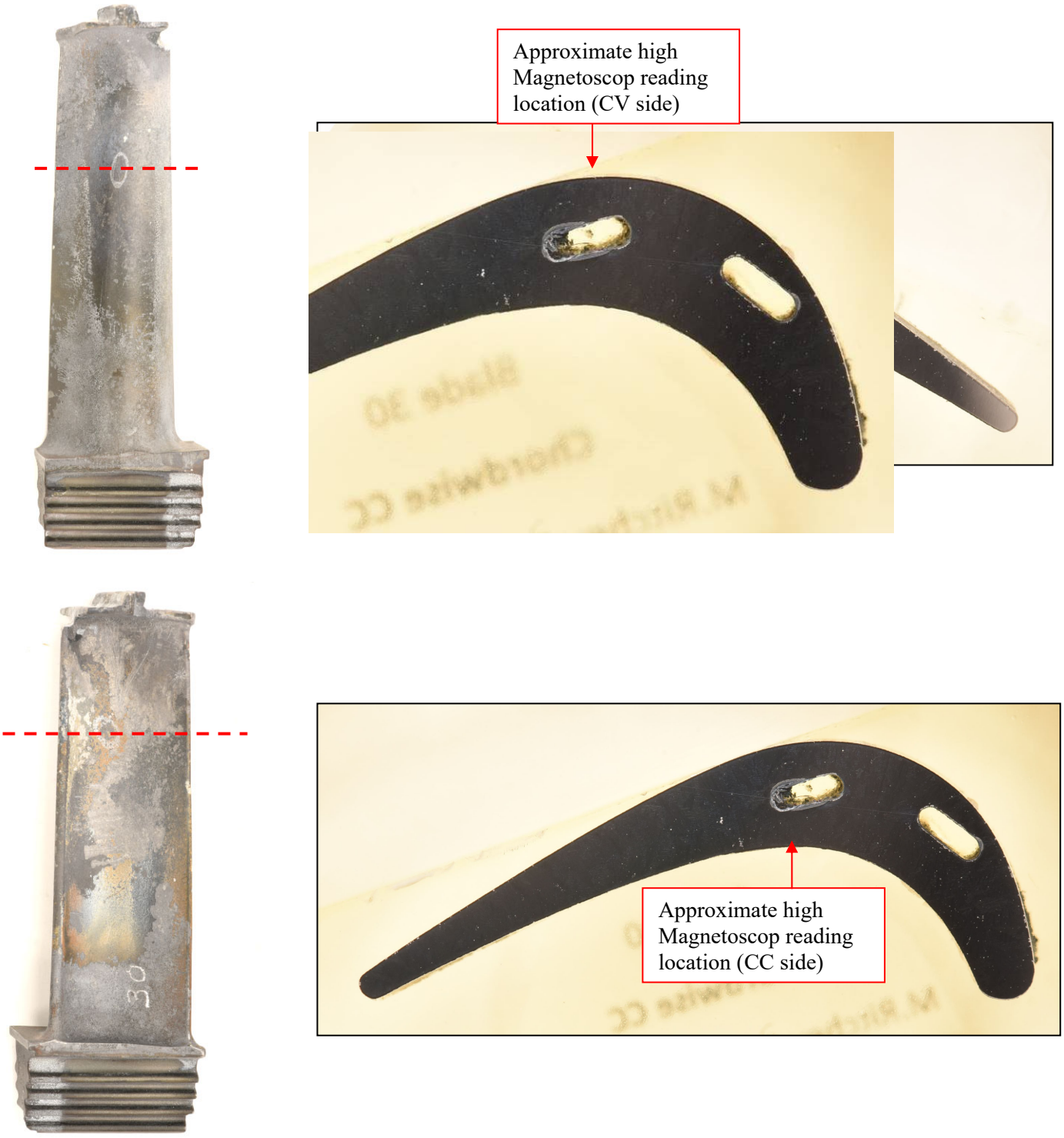

Figure 22: Images showing the locations of the metallographic sections prepared through the highest Magnetoscop readings on blade 30.

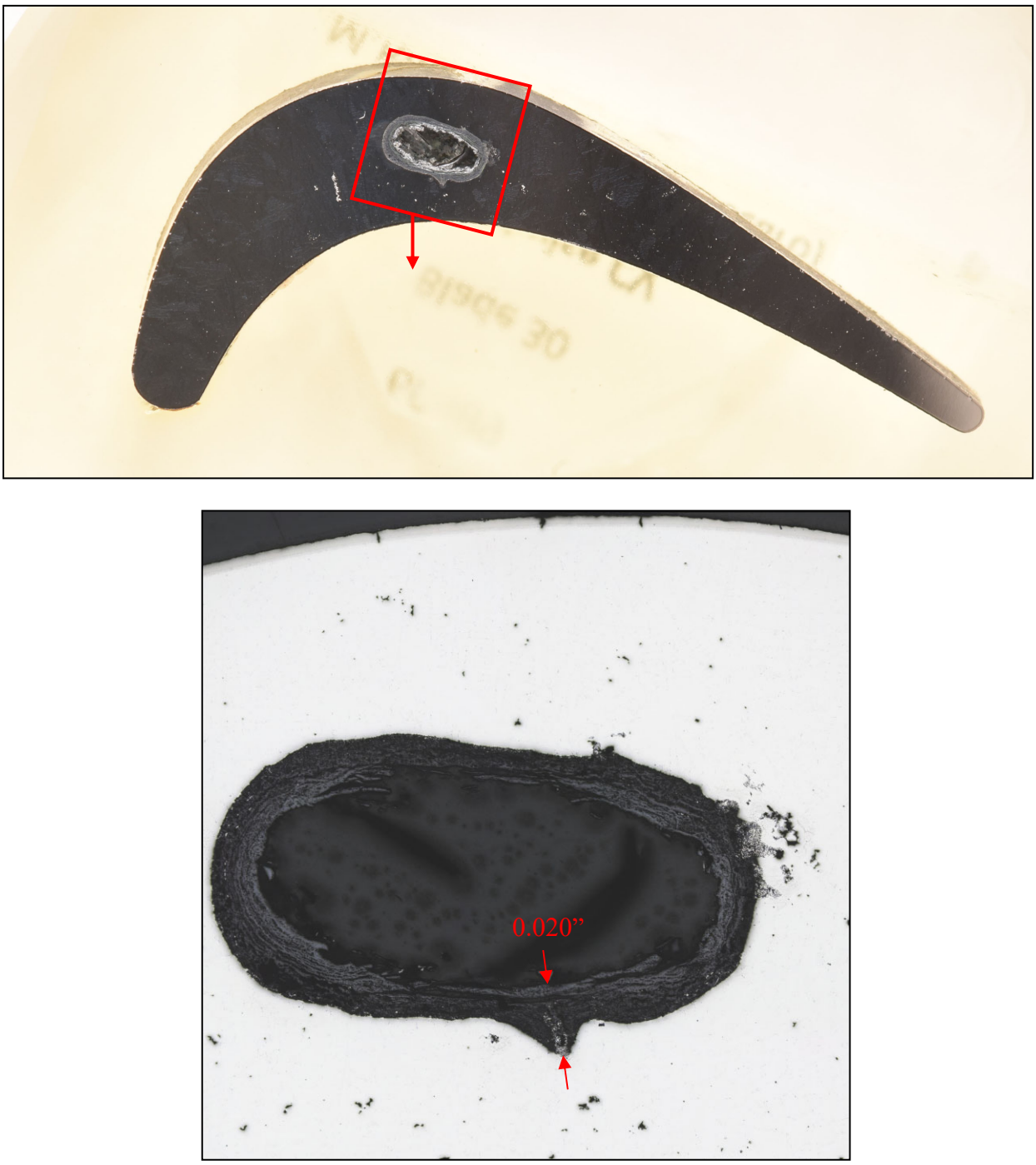

Figure 23: Metallographic review of the section through the convex side Magnetoscop location on blade 30 revealed corrosion on the internal hole up to 0.020” in depth. Only the hole at midchord was visible in the section.

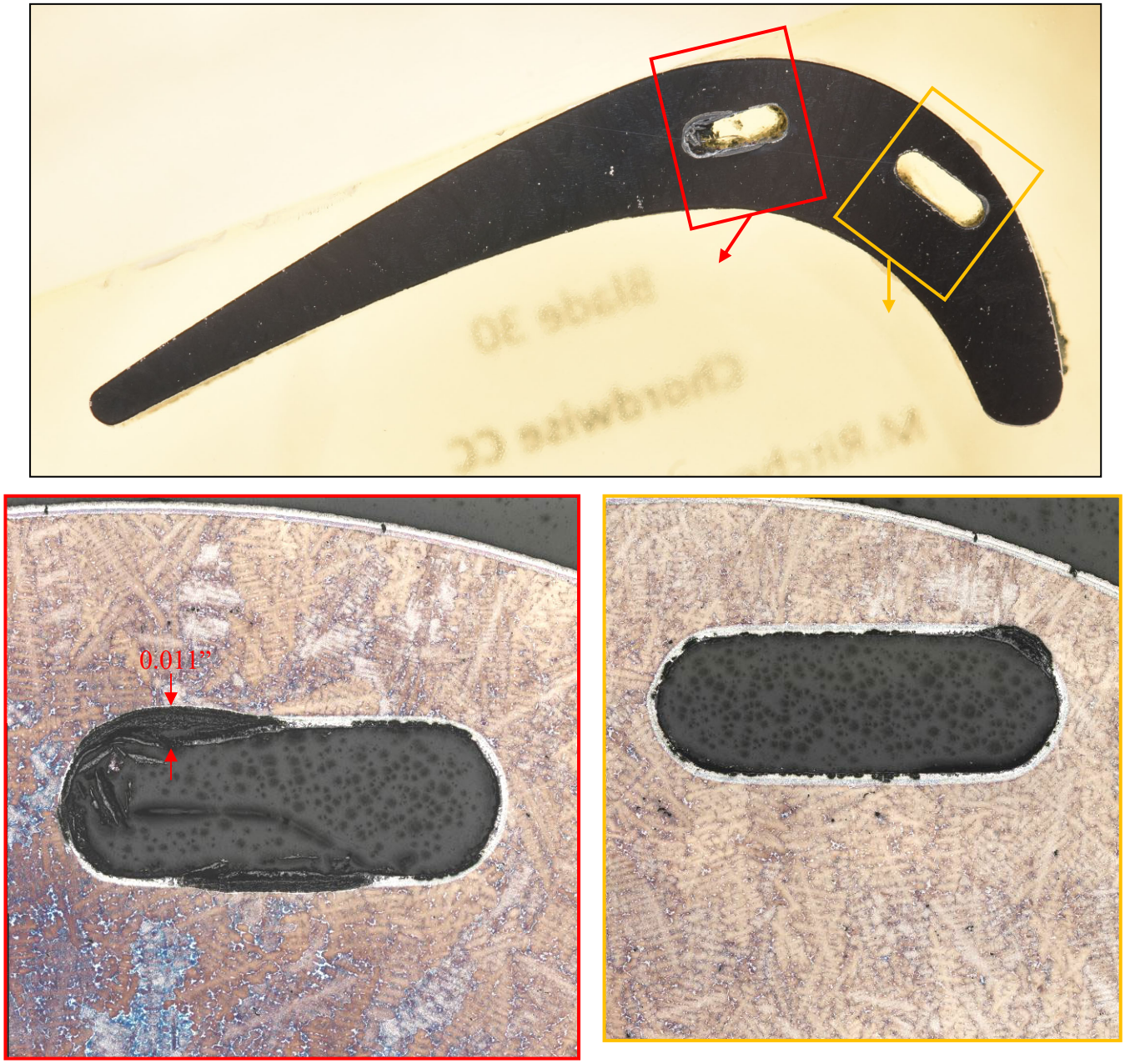

Figure 24: Metallographic review of the section through the concave side Magnetoscop location on blade 30 revealed oxidation/corrosion on the internal holes up to 0.011” in depth. The sample was etched with AG-21.

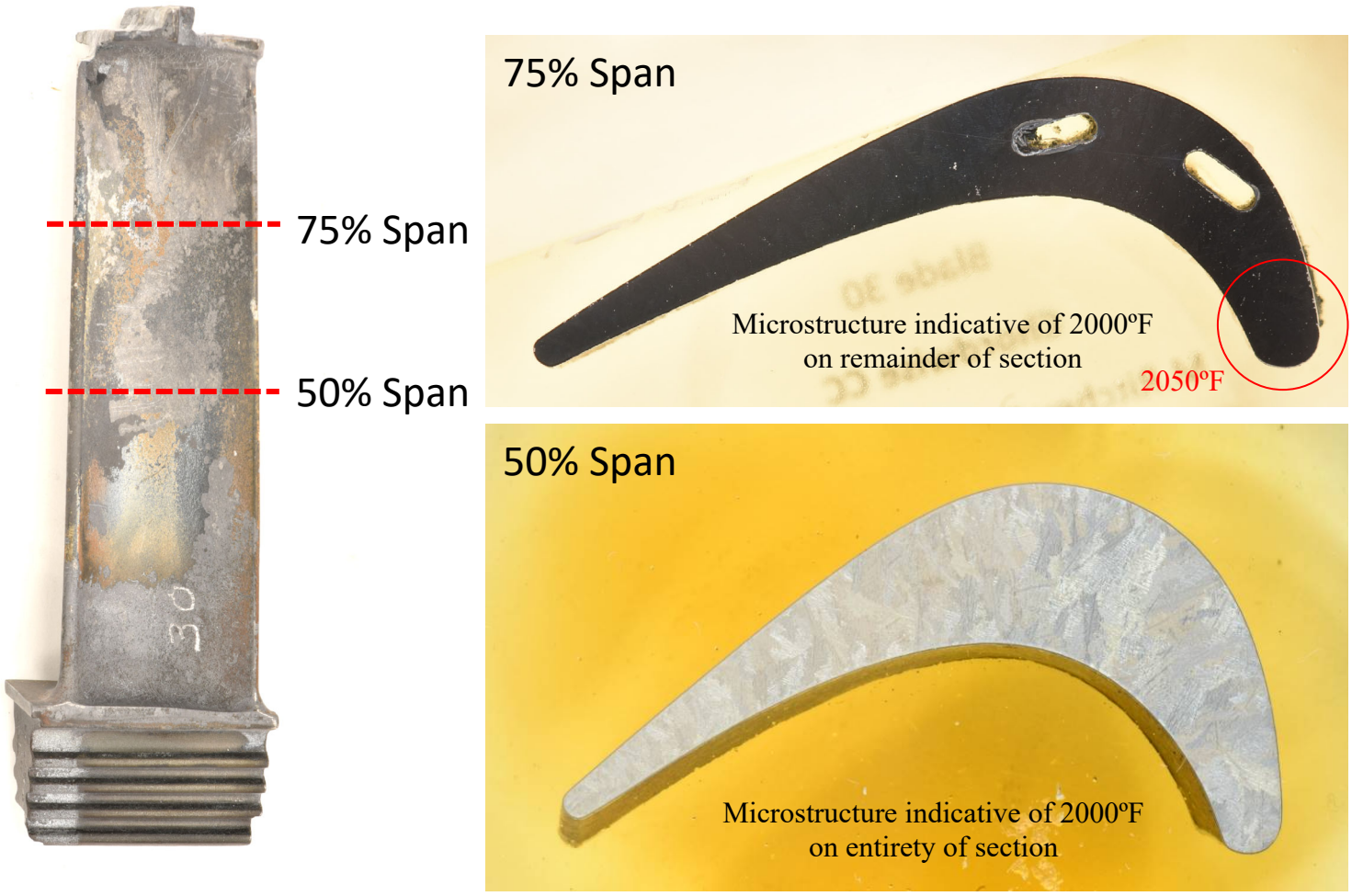

Figure 25: Metal temperature evaluation was completed at approximately 50% and 75% spans on blade 30. The microstructure in the airfoil at both 50% and 75% spans was indicative of temperature exposure of at least 2000ºF. Near the LE in the 75% span section, microstructure was indicative of temperature exposure of at least 2050ºF.

Figure 26: Closer views of blade 31 after cleaning, which was confirmed to be refurbished by TOS. Images showing the CC and CV sides as well as the part markings on the root and platform. Some of the part markings were illegible. The highest Magnetoscop locations on the concave and convex sides were circled by the NDE group.

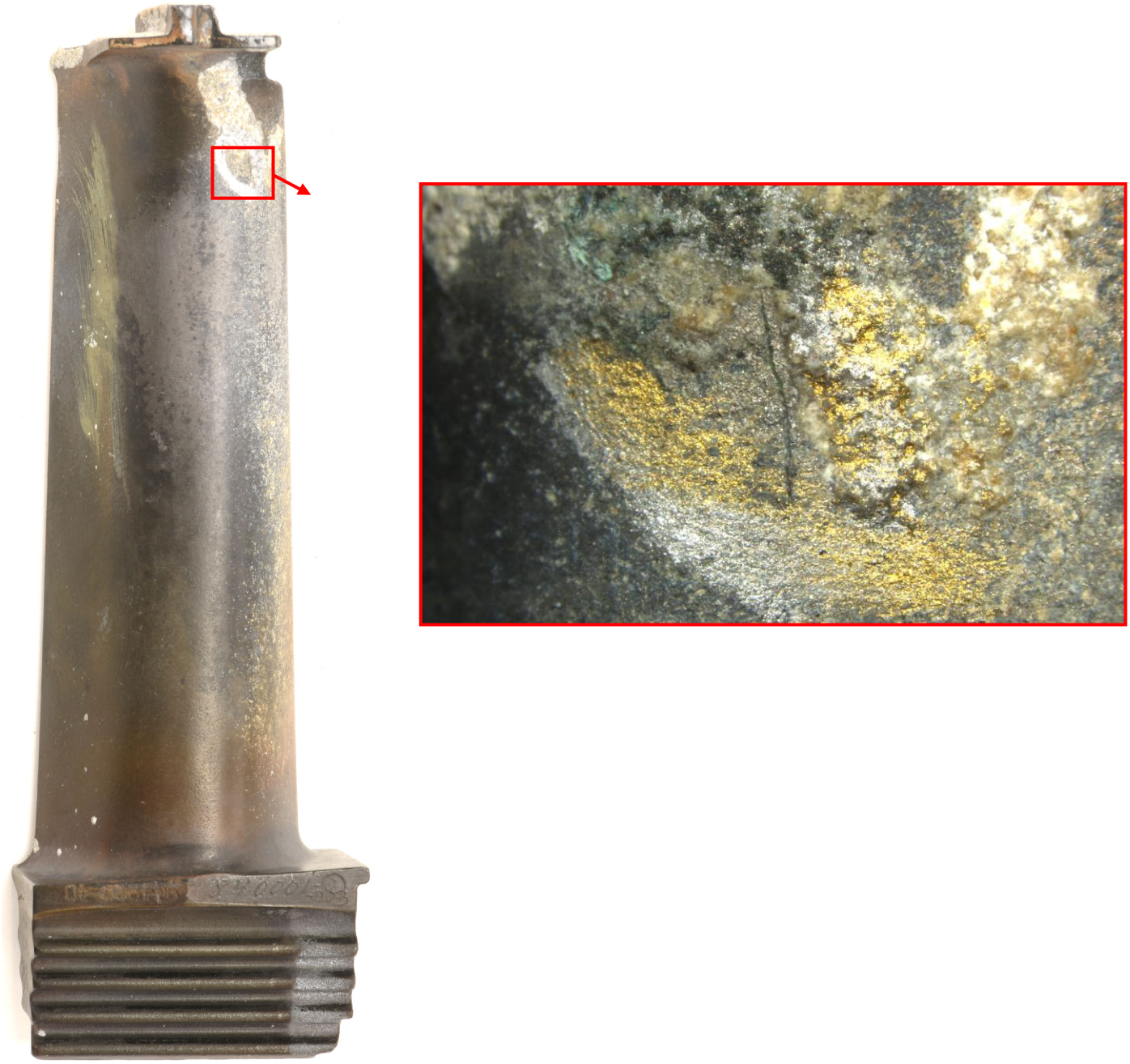

Figure 27: Image showing a spanwise crack-like feature at the Magnetoscop location on blade 31.

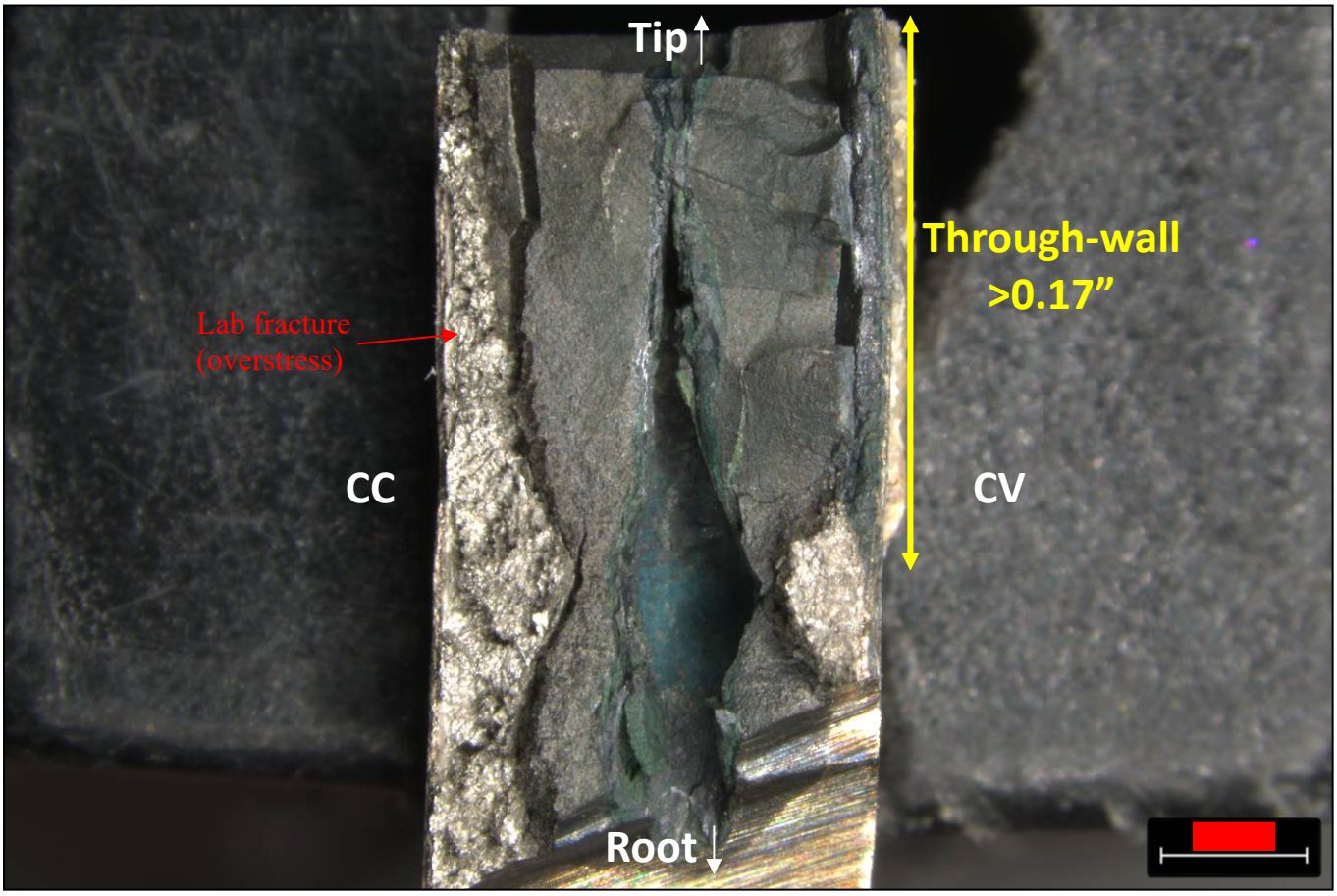

Figure 28: The spanwise crack-like feature was broken open. Extensive oxidation/corrosion was observed from the internal hole (dark-colored region). The discoloration extended through-wall for at least 0.17” along the convex surface.

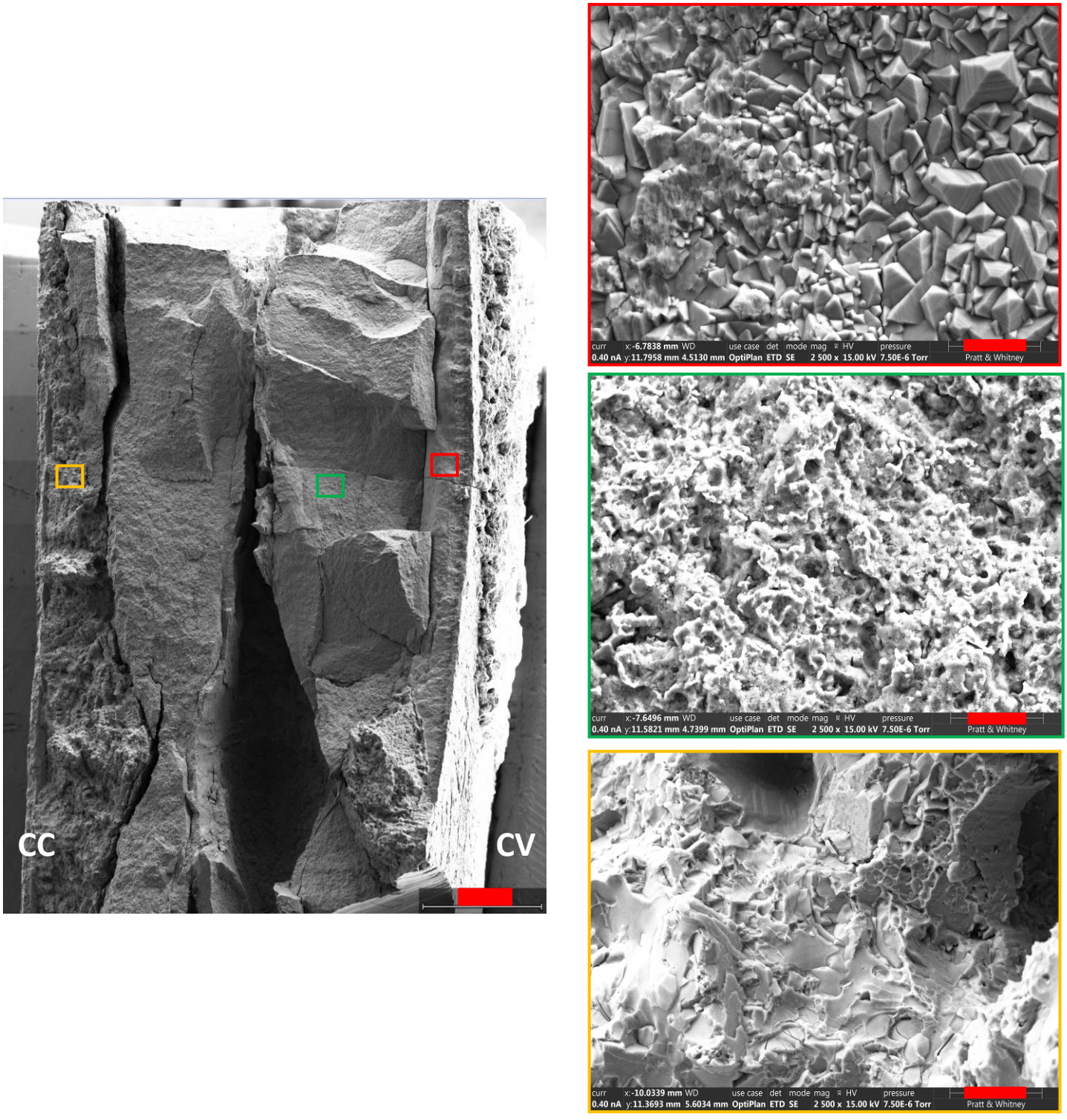

Figure 29: SEM examination identified features consistent with extensive oxidization/corrosion (top and middle images). The features along the concave wall were consistent with overstress from lab fracture (ductile dimples).

Figure 30: A metallographic section was prepared just outboard of the Magnetoscop location (outboard of where the crack-like feature was located). The locations of the highest convex and concave Magnetoscop readings were at approximately the same span so only one section was prepared.

Figure 31: Metallographic review of the section just outboard of the CC and CV Magnetoscop locations on blade 31 revealed oxidation/corrosion on the internal holes. On the hole closest to the LE, the oxidation/corrosion extended up to 0.043” through the CC wall, approximately 2/3 of the wall thickness. The oxidation/corrosion measured less than 0.007” on the hole closer to midchord.

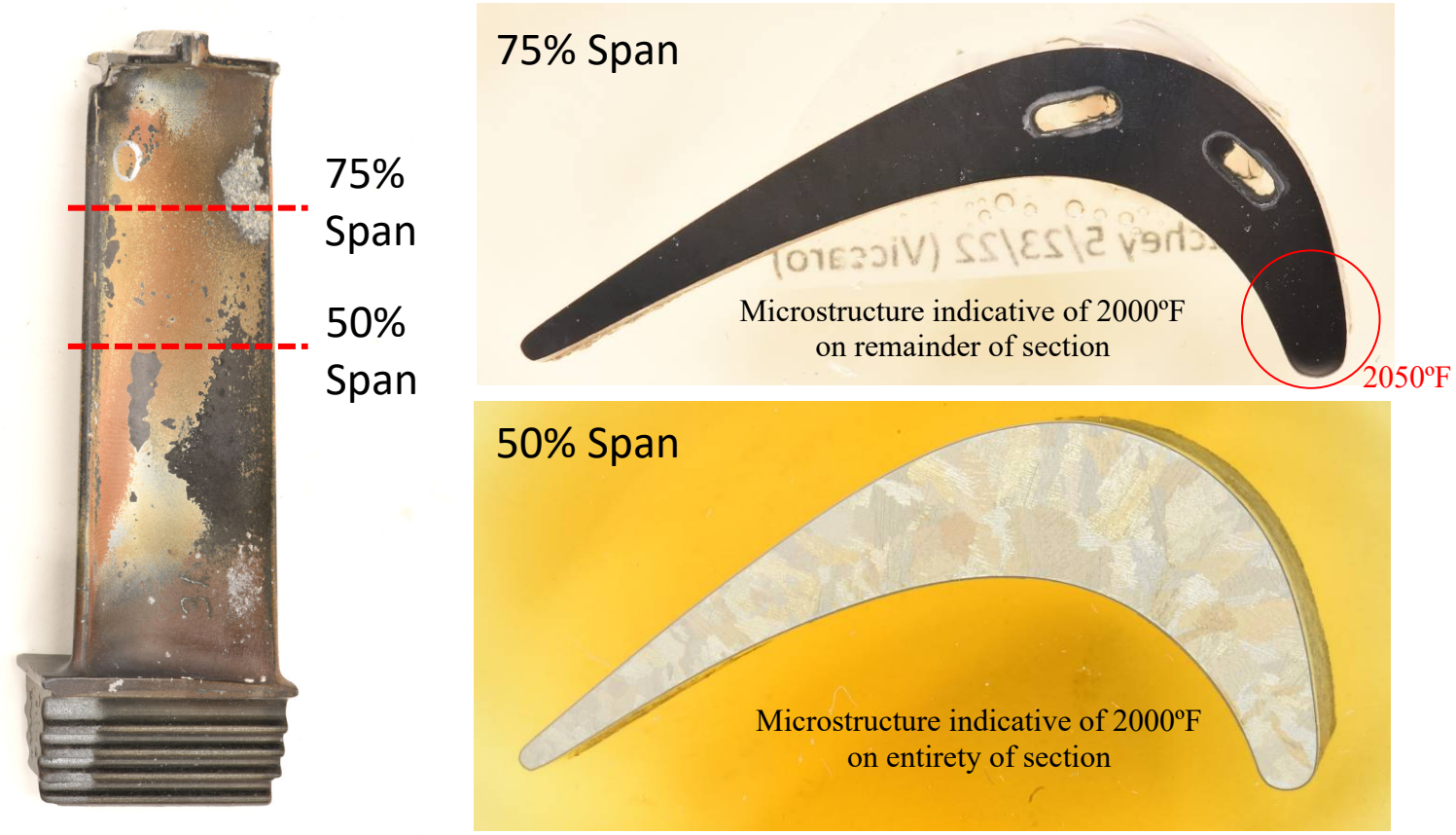

Figure 32: Metal temperature evaluation was completed at approximately 50% and 75% spans on blade 31. The microstructure in the airfoil at both 50% and 75% spans was indicative of temperature exposure of at least 2000ºF. Near the LE in the 75% span section, microstructure was indicative of temperature exposure of at least 2050ºF.

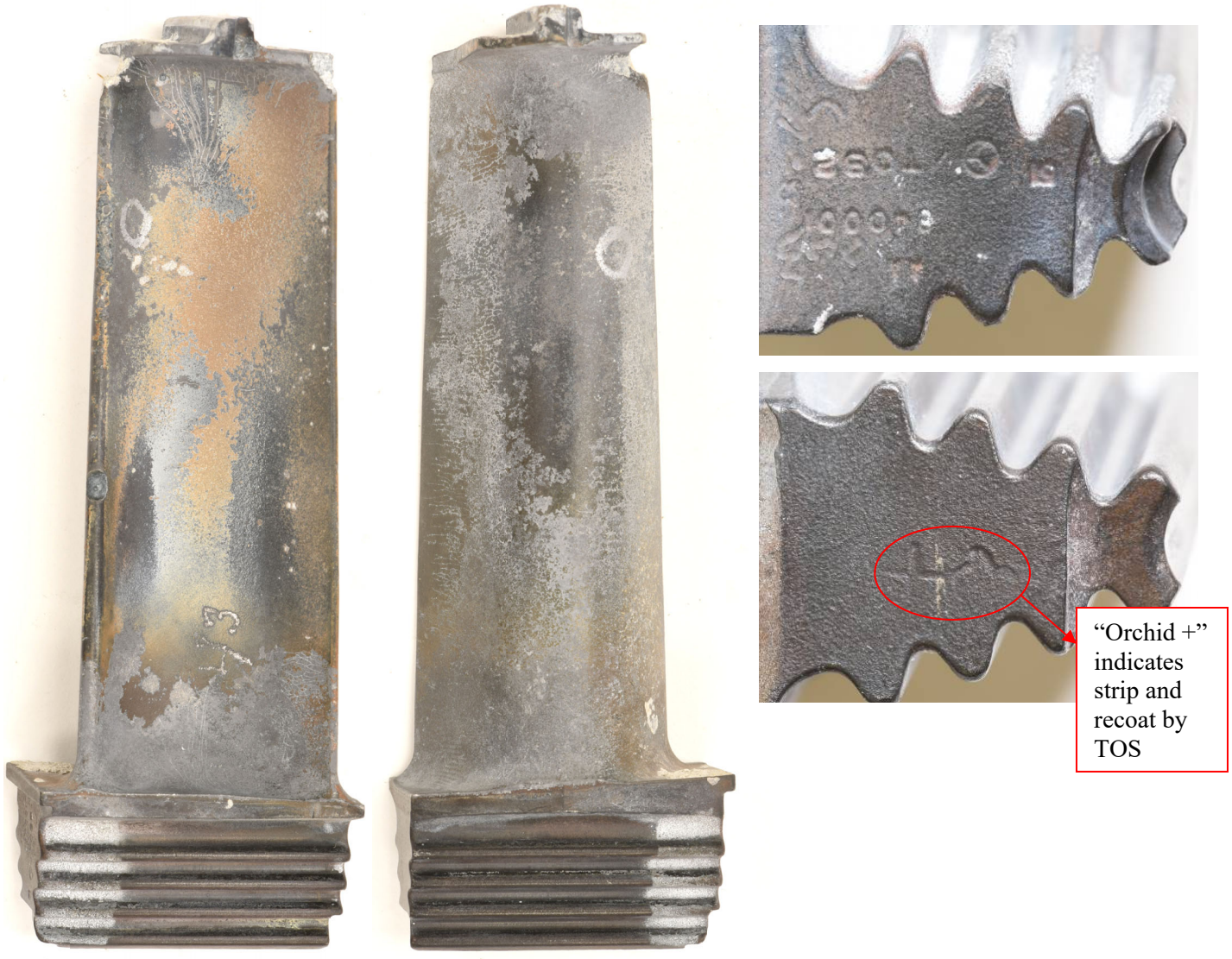

Figure 33: Closer views of blade 43 after cleaning, which was confirmed to be refurbished by TOS. Images showing the CC and CV sides as well as the part markings on the root. No part markings were visible on the platform. Some of the part markings were illegible. The highest Magnetoscop locations on the concave and convex sides were circled by the NDE group.

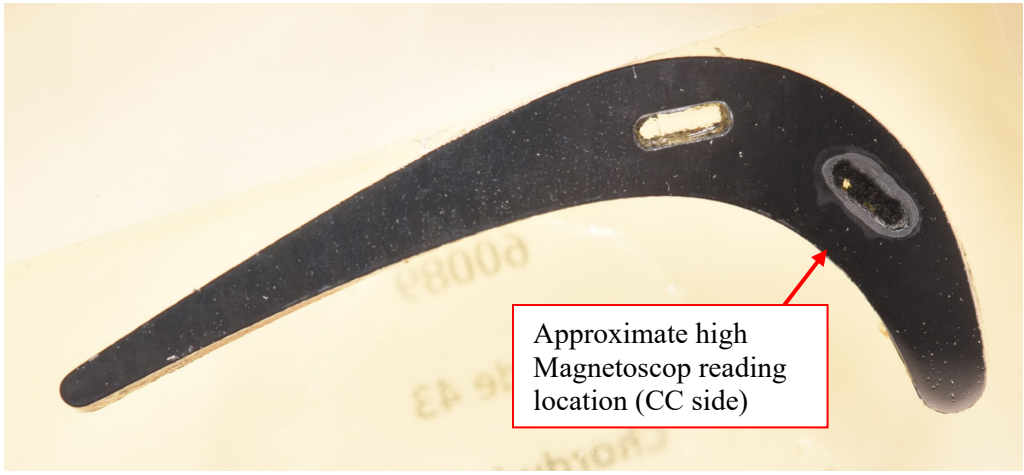

Figure 34: Images showing the locations of the metallographic sections prepared through the highest Magnetoscop readings on blade 43.

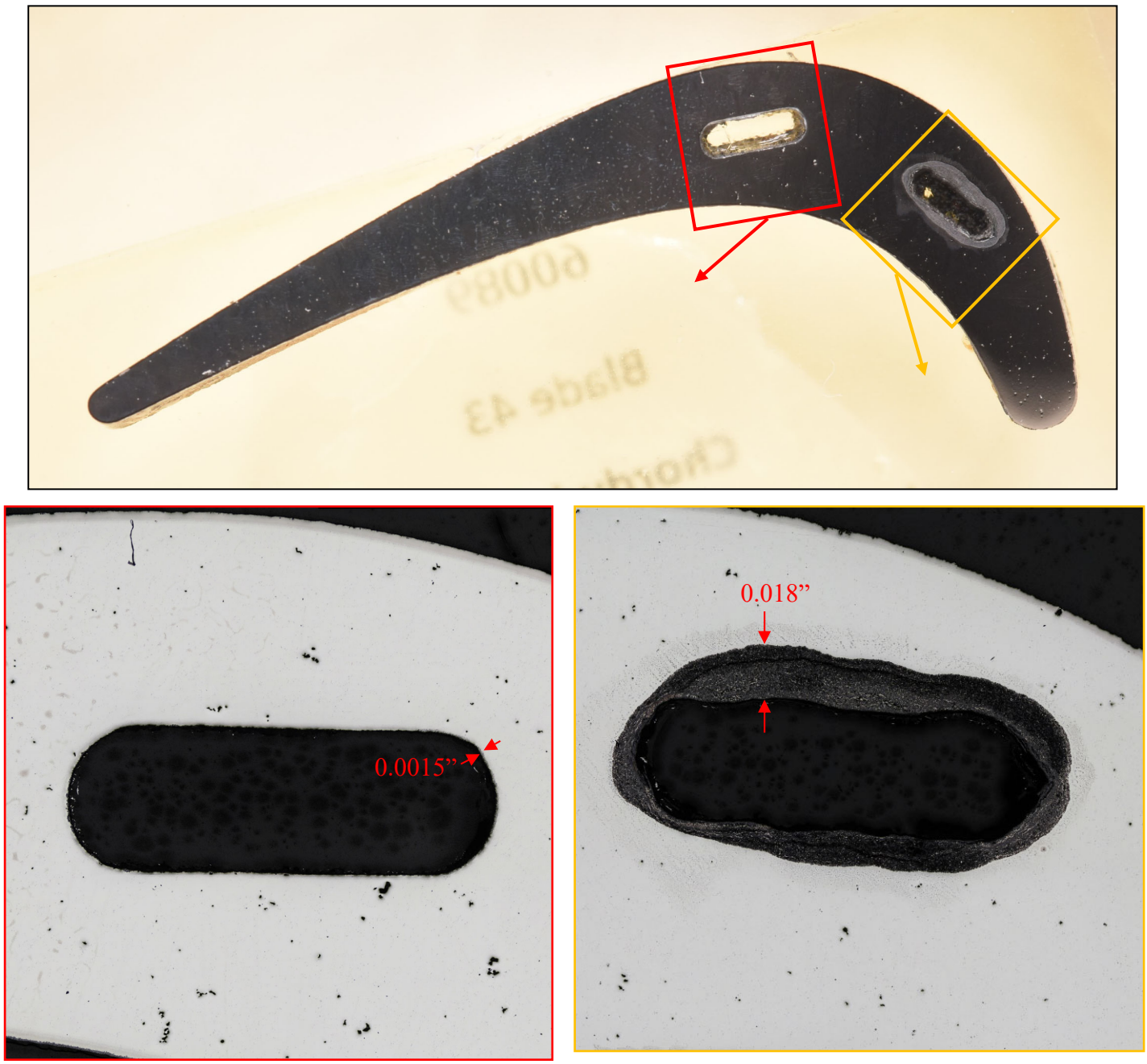

Figure 35: Metallographic review of the section through the concave side Magnetoscop location on blade 43 revealed oxidation/corrosion on the internal holes up to 0.018” on the hole closest to the LE, and 0.0015” on the hole near midchord.

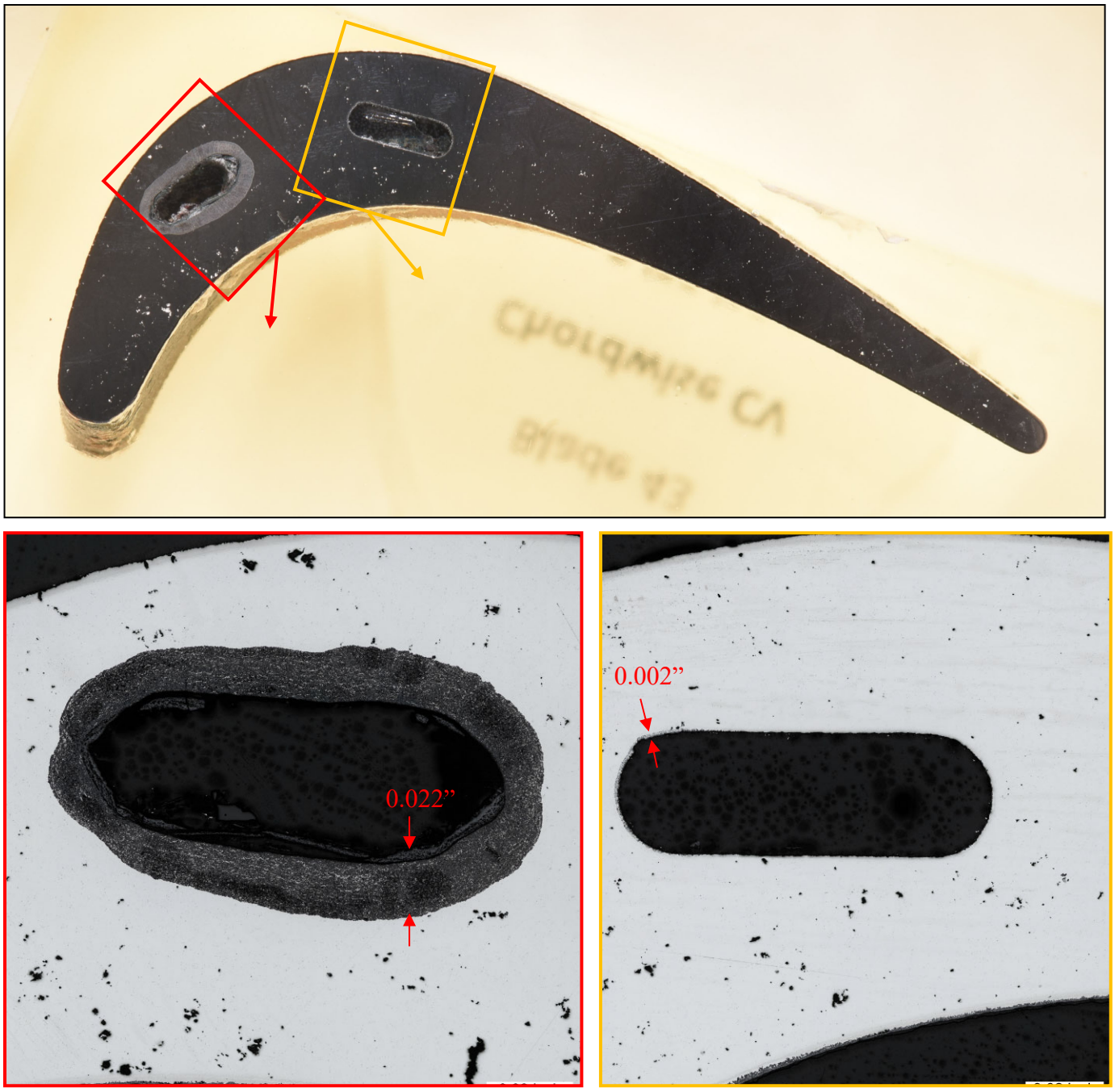

Figure 36: Metallographic review of the section through the convex side Magnetoscop location on blade 43 revealed oxidation/corrosion on the internal holes up to 0.022” on the hole closest to the LE, and 0.002” on the hole near midchord.

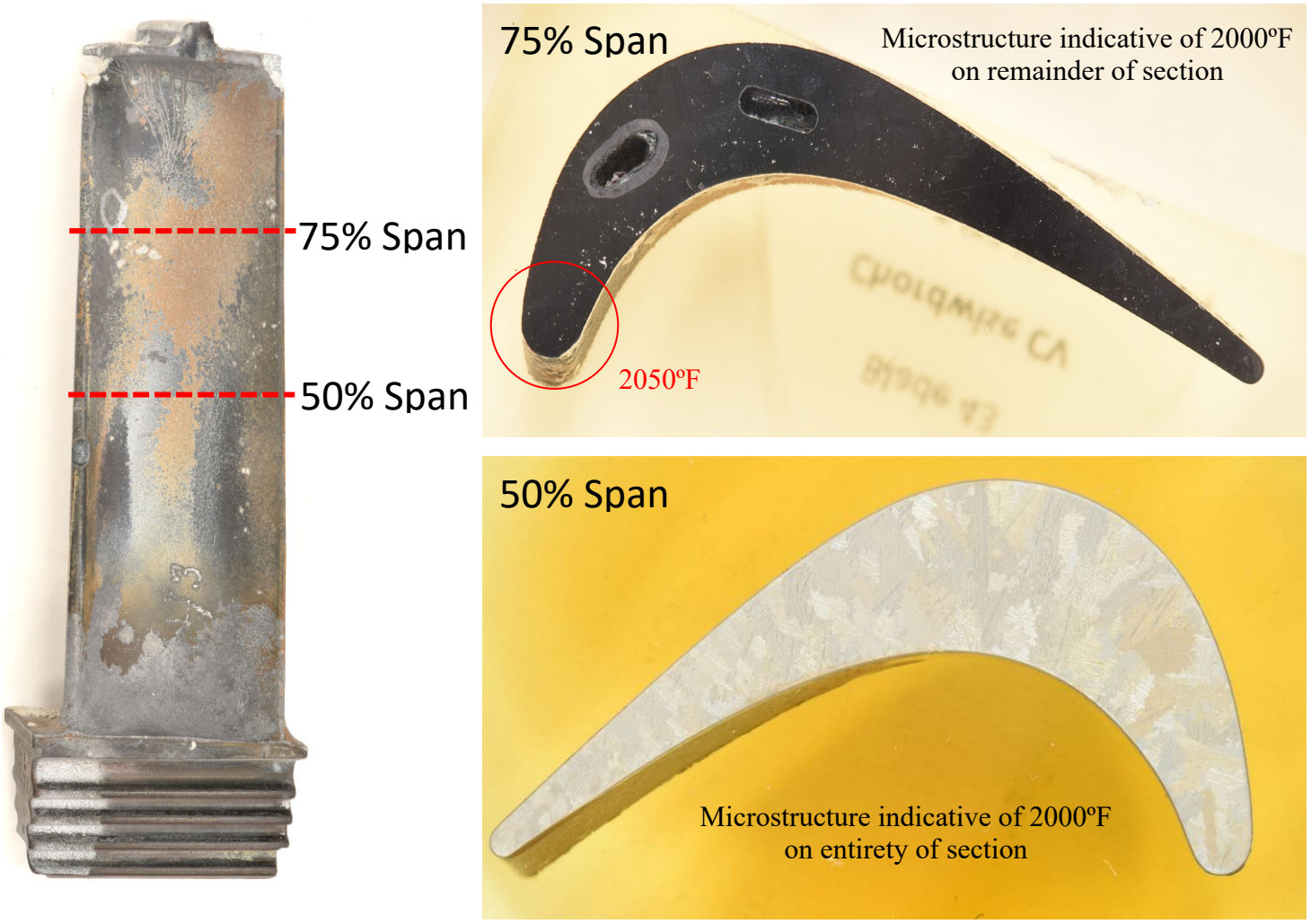

Figure 37: Metal temperature evaluation was completed at approximately 50% and 75% spans on blade 43. The microstructure in the airfoil at both 50% and 75% spans was indicative of temperature exposure of at least 2000ºF. Near the LE in the 75% span section, microstructure was indicative of temperature exposure of at least 2050ºF.

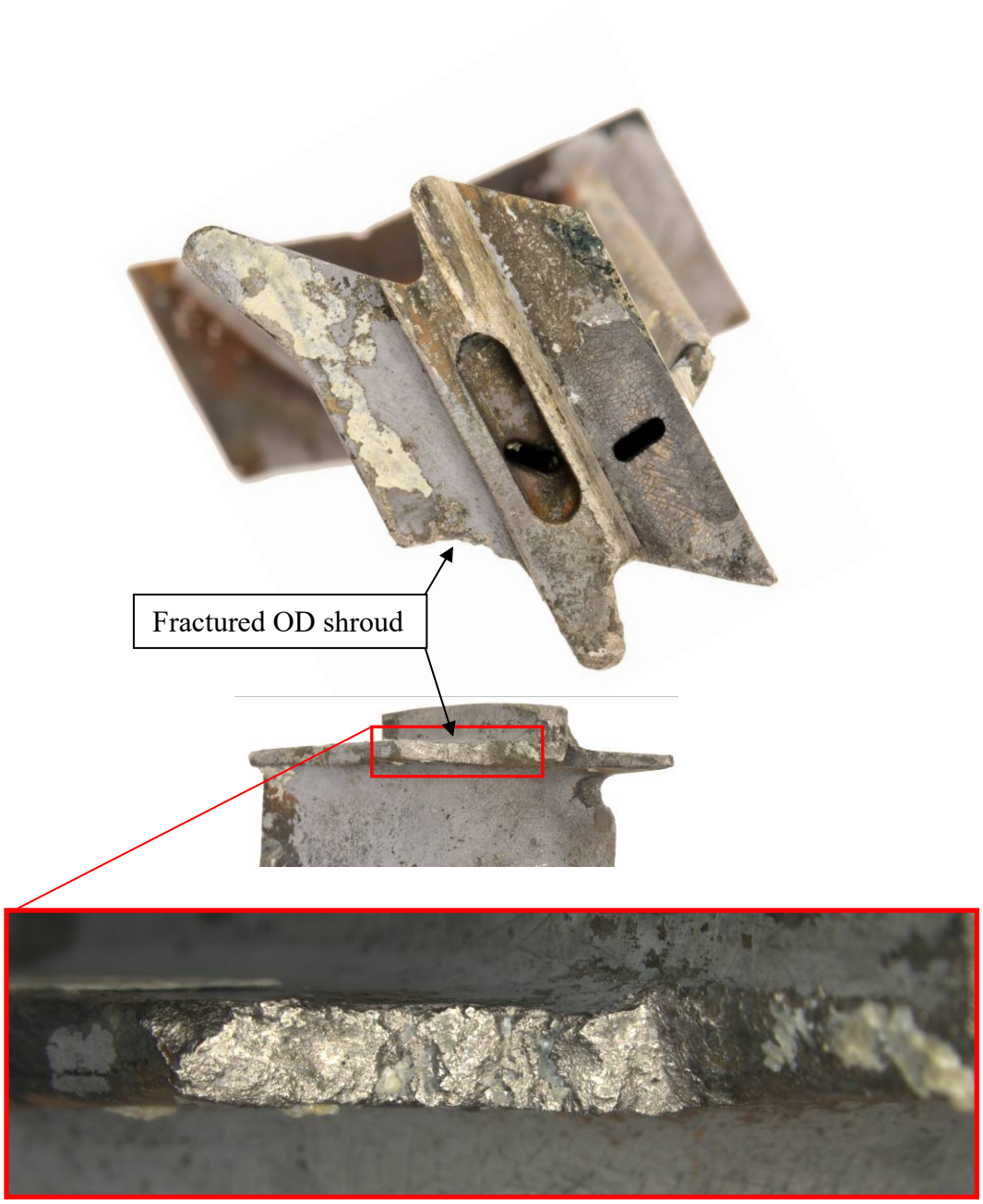

Figure 38: Blade 5 shroud fracture was rough textured and shiny, suggesting that it was due to overstress and was not exposed hot gases for much time.

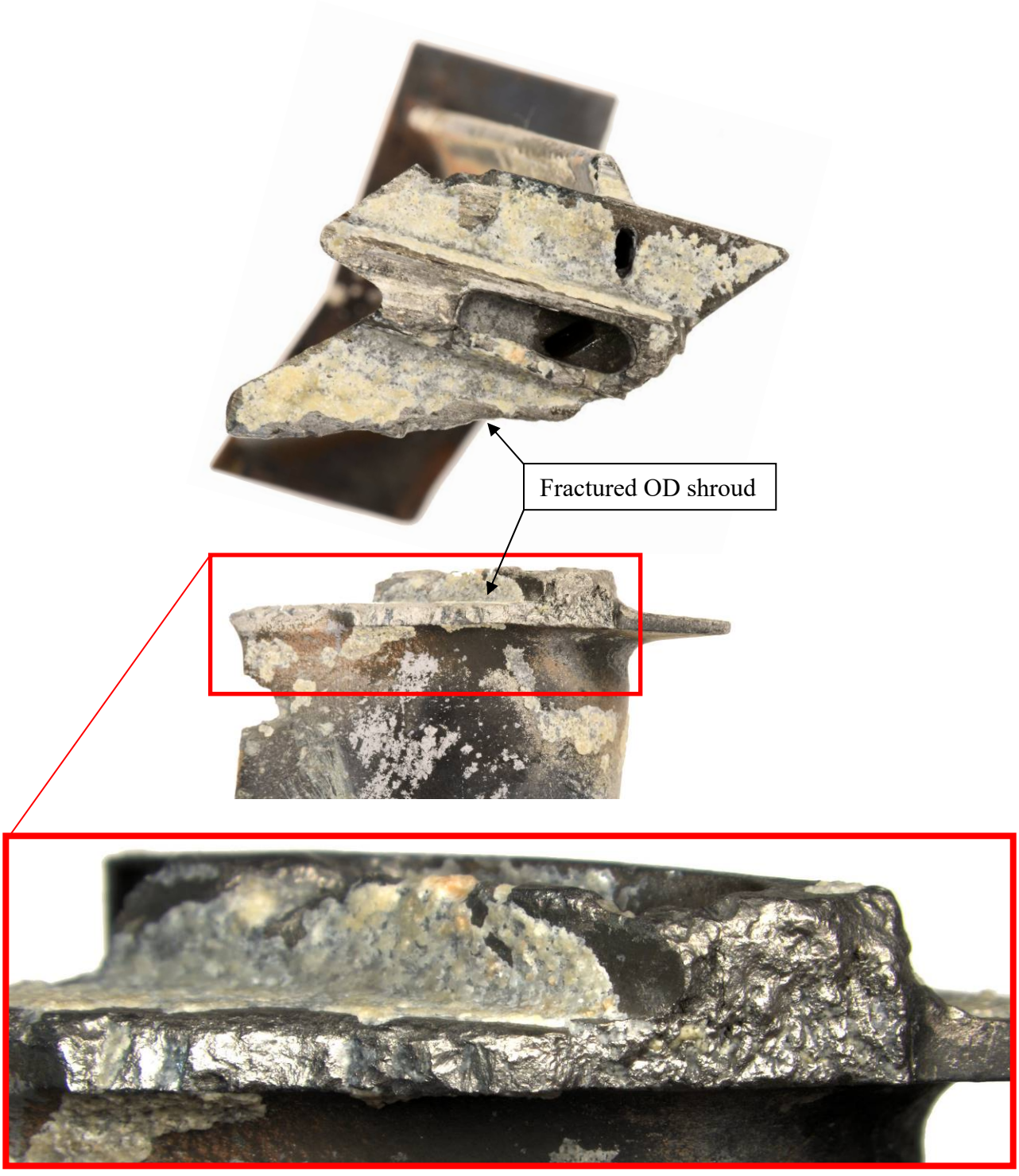

Figure 39: Blade 80 shroud fracture surface was rough textured and shiny, suggesting that it was due to overstress and was not exposed hot gases for much time.

Marking (Eng Pos)	Radial Creep	Rotational Creep
2	0.01	0.67098
3		0.60643
4	0.0165	
5	0.0092	0.84973
7	0.0146	-0.15243
8		
9	0.014	1.01142
10	0.0095	0.61749
11		
12		
13		0.56935
14	0.0112	0.86965
15	0.009	0.68581
16	0.0133	0.78639
17	0.0076	0.99796
18	0.0099	0.47057
19	0.013	
20	0.0125	0.47499
21	0.01	0.67703
22		0.84914
23	0.0108	0.60622
24	0.0244	
25	0.0111	0.96167
26	0.0131	0.77016
27	0.0158	0.70194
28	0.0028	0.42344
29	0.0145	0.12804
30	0.019	0.64648
31	0.008	
32	0.0074	0.81776
33	0.0153	
34	0.0157	0.23894
35	0.0089	0.89122
36		
37	0.0031	0.46278
38	0.017	0.66569
39	0.0083	0.08247
40	0.0076	

Marking (Eng Pos)	Radial Creep	Rotational Creep
41	0.0179	0.26787
42	0.0159	0.61971
43	0.0193	1.04853
44	0.0132	1.12238
45	0.0147	1.15506
46	0.0126	0.84612
47	0.0134	0.8803
48	0.0207	0.47263
49	0.0117	0.41095
50	0.0082	0.57729
51	0.0162	1.14195
52		1.12528
53		0.56591
54	0.0091	0.75792
55	0.0121	0.39346
56	0.0156	0.77223
57	0.0073	0.65587
58	0.0152	0.60596
59	0.0095	0.97291
60	0.016	0.69569
61	0	
63	0.0084	0.75664
64	0.0163	0.56277
65	0.0106	0.79572
66	0.0105	0.86462
67	0.0036	0.76269
68	0.0081	0.36579
69		
70	0.0111	0.62895
71	0.0085	0.84036
72	0.0151	0.69246
73	0.0068	0.6589
74	0.0169	0.4917
75	0.0054	0.50992
76		0.43157
77		
78	0.0157	0.96926
79		
80		

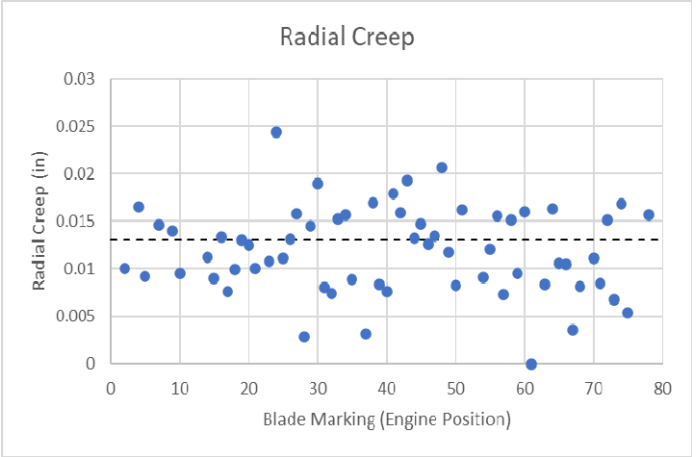

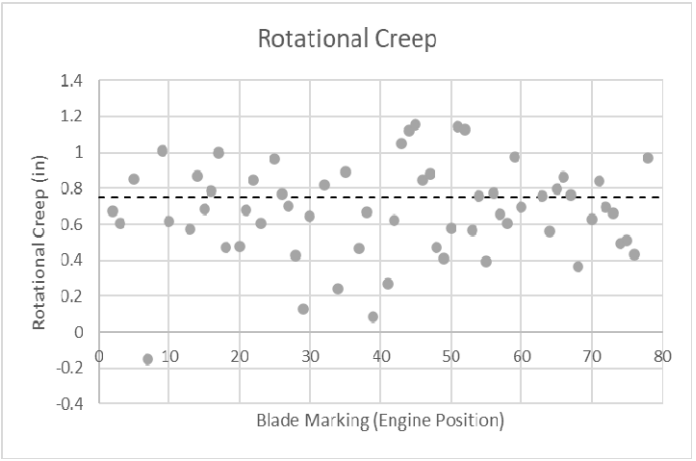

Appendix 1: Results of Non-Destructive Dimensional Inspections. Red text dimensions are rejectable to the engine manual. Orange text dimensions must be repaired per the engine manual. Blank cells could not be measured due to the interference of barnacles.

Blade #	Max µ 1.069	Max µ 1.070	Approx. Location
2	1.039	1.0186	CV LE tip
3	1.134	1.062	CV LE tip
4	1.005	1.019	CV LE tip
5	1.111	1.0531	CV LE tip
7	1.038	1.0018	CV tip center
8	1.005	1.0029	CC tip center
9	1.017	1.0082	CV LE tip
10	1.056	1.0271	CV LE tip
11	1.195	1.0836	CV Tip center
12	1.099	1.0517	CV LE tip
13	1.031	1.0161	CV Tip center
14	1.031	1.0155	CV midspan center
15	1.053	1.0295	CV midspan center
16	1.034	1.0113	CV midspan TE
17	1.002	1.0014	CV Tip center
18	1.009	1.0039	CV Tip center
19	1.003	1.0012	CV Tip center
20	1.024	1.0114	CV Tip center
21	1.005	1.0017	CV Tip center
22	1.227	1.1086	CV LE tip
23	1.007	1.0029	CV LE tip
24	1.003	1.0013	CV Tip center
25	1.013	1.0058	CV Tip center
26	1.009	1.0039	CV Tip center
27	1.01	1.0043	CV Tip center
28	1.002	1.0008	CV Tip center
29	1.004	1.0025	CV Tip center
30	1.007	1.0031	CV mispan center
31	1.117	1.0593	CV LE tip
32	1.042	1.0218	CV LE tip
33	1.027	1.0156	CV LE tip
34	1.005	1.0036	CV LE tip
35	1.005	1.0042	CV LE tip
36	1.159	1.0802	CV Tip center
37	1.065	1.0357	CV LE tip
38	1.076	1.0319	CV Tip center
39	1.052	1.0263	CV Tip center
40	1.007	1.0023	CV Tip center
41	1.084	1.0402	CV Tip center

Blade #	Max µ 1.069	Max µ 1.070	Approx. Location
42	1.033	1.0171	CV Tip center
43	1.071	1.0378	CV Tip center
44	1.057	1.0289	CV Tip center
45	1.003	1.0014	CV Tip center
46	1.005	1.0019	CV Tip center
47	1.146	1.0752	CV tip LE
48	1.06	1.0301	CV Tip center
49	1.003	1.0011	CV Tip center
50	1.041	1.0211	CV tip center
51	1.005	1.0025	CV tip center
52	1.143	1.0669	CV tip center
53	1.065	1.0316	CV tip center
54	1.048	1.0217	CV tip center
55	1.000	1.0013	CC midspan center
56	1.003	1.0006	
57	1.002	1.0008	CC tip center
58	1.005	1.0027	CV tip center
59	1.022	1.0104	CV tip center
60	1.031	1.015	CV LE tip
61	1.000	1.0000	n/a
62	1.155	1.0773	CV tip center
63	1.01	1.0034	CV tip center
64	1.014	1.0063	CV tip LE
65	1.007	1.0011	CV tip center
66	1.009	1.0042	CV tip center
67	1.005	1.002	CV tip center
68	1.018	1.0098	CV tip center
69	1.012	1.0066	CV tip LE
70	1.006	1.0037	CV tip LE
71	1.007	1.0032	CV tip LE
72	1.006	1.0025	CV Tip center
73	1.053	1.0255	CV tip LE
74	1.100	1.0467	CV tip center
75	1.007	1.002	CV tip center
76	1.009	1.0019	CV tip center
77	1.011	1.0041	CV tip LE
78	1.057	1.025	CV tip center
79	1.026	1.0116	CV tip LE
80	1.005	1.002	CC tip center

Appendix 2: Magnetoscop inspection results. The engine manual acceptance limit for the 1.069 model is 1.06. Seventeen blades measured 1.06 or greater (highlighted). No limits have been established for measurements made with the 1.070 model Magnetoscop.